Engineered Science
DOI: https://dx.doi.org/10.30919/es1137

Buckling of Thin-Walled Stiffened Panels in Transportation Structures: Benchmarking and Parametric Study

Adrevee Ronald Kusuma Sarwoko,[1] Aditya Rio Prabowo[1,*] Tohid Ghanbari-Ghazijahani,[2] Quang Thang Do,[3] Ridwan Ridwan,[4] Muhammad Imaduddin Hanif[5]

Abstract

The increasingly frequent utilisation of aircraft across the globe significantly increases the likelihood of structural failures. One contributing factor to aviation accidents, as revealed by the International Civil Aviation Organization (ICAO) and Indonesian National Transportation Safety Committee (KNKT) investigation, is technical errors stemming from structural failures in aircraft. Buckling in thin-walled structures leads to a substantial increase in deformation and a subsequent reduction in load-bearing capacity. To address this, lightweight and high-strength stiffener panels are employed. This study focuses on investigating the buckling resistance of stiffened aircraft panel structures. The finite element method is utilised to numerically simulate and analyse the stiffened panels under predetermined boundary conditions. Three main types of variations are considered: (i) stiffener type within the controlled volume, (ii) number and spacing of stiffeners in the panel, and (iii) stiffener configuration. The adopted material for the stiffener panels is 2024-T3 aluminium alloy, with panel geometry resembling that of a reference model. The findings demonstrate that adopting a Y-shaped stiffener geometry, incorporating transverse stiffeners, and reducing the distance between stiffeners enhance the buckling resistance and collapse performance of the stiffened panel structure.

Keywords: Transportation; Finite element method; Thin-walled structure; Stiffened panels; Buckling.
Received: 16 December 2023; Revised: 16 January 2024; Accepted: 05 February 2024.
Article type: Research article.

1. Introduction

Aviation is a complex system that includes the use of airspace, aircraft operations, airport management, air transportation services, flight navigation protocols, safety and security measures, environmental considerations, and supporting facilities. It is a multi-faceted system that works together to ensure the efficient functioning of air travel and transportation, encompassing various activities and sectors that contribute to the advancement of the aviation industry. Aviation activities play a crucial role in facilitating human mobility within a country. However, the increased frequency of aircraft usage in Indonesia has raised concerns about the potential for more severe accidents.[1] According to the International Civil Aviation Organization (ICAO), an aircraft accident refers to an incident that transpires from the time an aircraft prepares for take-off until it comes to a complete stop after the flight, with criteria including casualties, serious injuries, damage or structural failure to the aircraft, and complete loss or inaccessibility of the plane. As depicted in Fig. 1(a), countries in Asia, Europe, and America are the major locations of fatal civil airline accident occurrences, of which the United States is at the top of the list. In terms of the flight phase (Fig. 1(b)), landing is the most dangerous phase with more than 200 occurrences of accidents. On a global scale, as presented in Fig. 1c, the fatal accident rate has risen since 2021, with this trend observed in both regional and state scopes.[2-4] On the

[1] *Department of Mechanical Engineering, Universitas Sebelas Maret, Surakarta 57126, Indonesia.*
[2] *Department of Civil Engineering, Macquarie University, Sydney 2109, Australia.*
[3] *Department of Naval Architecture and Ocean Engineering, Nha Trang University, Nha Trang, 650000, Viet Nam.*
[4] *Department of Mechanical Engineering, Universitas Merdeka Madiun, Madiun 63133, Indonesia.*
[5] *Laboratory of Design and Computational Mechanics, Faculty of Engineering, Universitas Sebelas Maret, Surakarta 57126, Indonesia.*
**Email:* aditya@ft.uns.ac.id (A. R. Prabowo)

© Engineered Science Publisher LLC 2024

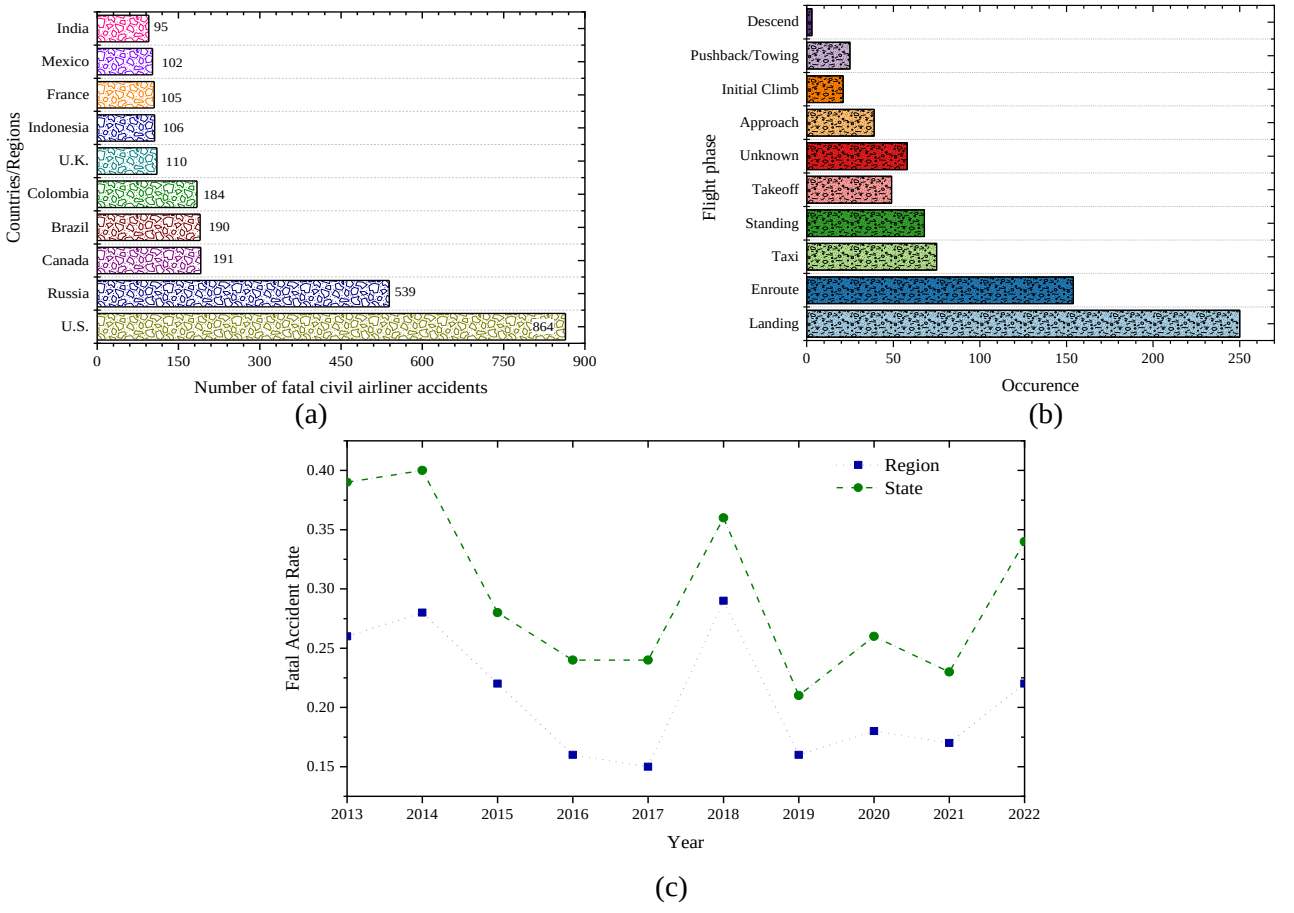

Fig. 1 Compiled aircraft accident data based on: (a) Top 10 countries; (b) flight phase; and (c) scope.

other hand, at the country level, based on the period between 2018 and 2022, the National Transportation Safety Committee (KNKT) of the Republic of Indonesia investigated a total of 140 aviation accidents, encompassing both accidents and serious incidents. In 2022 alone, the KNKT investigated 20 incidents.[3] The KNKT's investigations have identified several factors that contribute to aviation accidents; namely, human, technical, environmental, and facility-related factors.[5] Technical failures can arise due to various factors, including structural failures within the aircraft itself.

In the context of aviation, structural failure is the inability of a component or part within an aircraft or the aircraft itself to withstand the loads it is subjected to, resulting in a loss of loading capacity. The onset of structural failure arises when a material is subjected to stress beyond its strength limit, resulting in excessive deformation. It is imperative in structural engineering and design to consider and address the possibility of ultimate failure strength. The structural components of an aircraft hold paramount importance, as they endure diverse flight loads throughout their service. Past incidents serve as cautionary tales, highlighting the significance of maintaining the integrity of safety-critical structural elements to prevent consequential harm to both humans and aircraft. Hence, it is crucial to comprehend the characteristics of the aircraft structure, the loads they are subjected to, and the different types of failures that may occur. Such knowledge can aid in developing remedial actions to prevent such incidents.[6]

The failure of aircraft components can arise from various sources, including design errors,[7] microstructure defects,[8] loading conditions (such as overload and fatigue),[9] human error, and environmental factors.[10,11] One common area where failures occur in aircraft structures is thin-walled structures, which serve as load-bearing components. In these structures, buckling failure leads to a significant increase in deformation, resulting in a loss of load-bearing capacity.[12,13] Thin-walled structures have found widespread application across different industries, such as offshore drilling rigs, ships, airplanes, submarines, bridges, nuclear reactors, and rooftop units. These structures often experience compression loads that exceed their critical limits, leading to plate buckling. To address this issue, stiffened elements are employed due to their lightweight nature and high strength. Mechanical failures in components can result from non-uniform in-plane loads.[14] Stiffener-reinforced plates play a vital role in aeronautics and space shuttle vehicles.[15] Plates can fail under various conditions,

 © Engineered Science Publisher LLC 2024

including corrosion-induced failure,[16] yield point cracks,[17] impact loads,[18-20] and buckling.[21] Buckling occurs when a plate abruptly bends under a compression load. Given that stiffener panels offer simplicity in terms of fabrication and possess a high strength-to-weight ratio, a precise understanding of the behaviour and conditions of these structures under extreme loading is essential for ensuring optimal design limits.

Stiffener panels, despite their challenging manufacturing process and high computational cost, remain in high demand within sectors such as the aircraft industry. Even minor local geometric flaws in metallic components can lead to reduced buckling capacity, ultimately resulting in failure.[22] Experimental research has revealed various limitations including material characteristics, failure criteria, structural distortions during manufacturing and assembly of models, maintenance levels, and other factors, making these components highly complex.[23] However, the advancement of computer technology has paved the way for conducting research using numerical methods, specifically Finite Element Analysis (FEA), which is both practical and cost-effective. FEA enables researchers to overcome the challenges associated with complexity.[24] Through employing the Finite Element Method (FEM) in FEA, researchers can determine the structural responses and behaviours related to buckling failure.

The objective of this research is to enhance the buckling resistance of stiffened panel structures in aircraft through effectively addressing the challenges posed by compressive axial loads. To achieve this, simulation of the buckling behaviour of an aircraft structure was conducted, and the results were validated through benchmarking against experimental tests. Considering a range of numerical and physical parameters, the investigation aimed to determine the optimal design of the aircraft structure, providing superior performance in terms of resisting buckling. Various numerical and physical parameters of the reinforced panel structure were analysed to identify the optimal design for an aircraft structure with enhanced resistance to buckling. The study incorporated four types of stiffeners: (a) Type-I, (b) Type-L, (c) Type-T, and (d) Type-Y. The use of numerical simulation is gaining popularity due to its cost-effectiveness, in accordance with contemporary demands. It is crucial to acknowledge that the study's limitations included the exclusion of welding effects on the stiffeners.

2. Highlights on related works

Collapse behaviour due to buckling loads can be determined using both numerical and analytical methods. Researchers have utilised these approaches to investigate various aspects of buckling behaviour in structures as summarised in Table 1. Nonami *et al*.[25] employed a calculation method to optimise the stiffener plate, evaluating its structural strength without relying on finite element modelling. Durban *et al*.[26] conducted research on the elastoplastic buckling of square plates, considering different boundary conditions and utilising analytical and numerical methods to explore the variation in the a/b ratio. Balenkiy *et al*.[27] employed non-linear finite element analysis to determine the ultimate load of a stiffener ship structure subjected to lateral loads. Danielson *et al*.[28] performed a study utilising numerical and analytical methods to assess the buckling behaviour of a square plate with a flat bulb stiffener installed on one side. Similarly, Kwon *et al*.[29] investigated the effects of longitudinal stiffeners on the buckling loading behaviour of stiffened panels. Prabowo *et al*.[30] analysed the buckling loads on supported rectangular plates, examining the influence of plate thickness, stiffener thickness, and sub-stiffeners. They observed a significant increase in strength with increasing plate and stiffener thickness, while the thickness of sub-stiffeners had an insignificant effect.

The collapse behaviour resulting from buckling has garnered significant research attention for over two decades, with extensive studies focusing on the behaviour of plates and stiffened panels.[30] Researchers such as Seifi and Khoda-yari[31] and Sujiatanti *et al*.[32] have investigated the impact of cracks on critical buckling load and ultimate collapse load, concluding that cracks reduce load capacities. In 2011, Xu *et al*.[21] studied the ultimate strength of stiffened panels using three types of stiffeners (flat, angle, tee bar).

In the study by York,[34] it was demonstrated that symmetric designs are unable to achieve superior buckling performance, when compared to non-symmetric designs. Furthermore, Peng *et al*.[35] found that changes in skin thickness have a greater impact on the buckling load compared to the ultimate load. Mantzaroudis and Stamatelos[33] analysed the approximation of closed-form buckling solutions for local skin buckling of stiffened plates with omega-type stringers. These findings highlight a research gap in the field of structural engineering; namely, the lack of comprehensive studies on the influence of different types and designs of stiffeners on the buckling behaviour of thin-walled structures. Therefore, it is crucial to investigate how various stiffener configurations can enhance the buckling resistance and performance of thin-walled structures in various applications, particularly in the context of the newest stiffener models.

3. Plate buckling and their theoretical concept

The buckling phenomenon occurs when structural

© Engineered Science Publisher LLC 2024

Table 1. Summary of the pioneer works related to stiffened panels and buckling.

Authors / Reference	Year	Research Methodology	Research Topic/Title	Research Object	Findings and Remarkable Notes
Durban *et al.*[26]	1999	Analytical method	Buckling of rectangular plates under biaxial loading	Rectangular plate	The predictions based on flow theory consistently yield higher values compared to the results obtained from deformation theory. As transverse tension and plate thickness increase, the disparity between the buckling stresses calculated using the two theories also grows.
Balenkiy *et al.*[27]	2001	Numerical method (Finite Element Method)	Ultimate load on structural members subjected to lateral loads	Beams	Using limit analysis theorems, the strength of stiffened ship structures under lateral loads can be assessed by comparing them with the ultimate loads.
Danielson *et al.*[28]	2004	Analytical, Numerical method, and Experiment	Stiffened plates' buckling with bulb-flat flanges	Stiffened panels with bulb stiffener	The investigation produced several outcomes, such as formulas for the planar properties of the flange geometry with asymmetry, a formula for the torsional constant of the flange cross section based on Saint-Venant theory, and a formula for the stress that causes the structure to buckle in a tripping mode.
Kwon *et al.*[29]	2011	Experiment	Compression tests of longitudinally stiffened plates undergoing distortional buckling	Stiffened panels	Regardless of whether the dominant buckling mode is distortional or a combination of local and distortional buckling, longitudinally stiffened plates exhibit a notable reserve of post-buckling strength when these buckling modes interact.
Seifi and Khodayari[31]	2011	Experiment and Numerical method	Cracked thin-plates	Thin plates	As the crack length increases, the buckling load decreases. The buckling load is more sensitive to the crack length when the cracks are aligned with the loading direction than when they are not. As the crack inclination angle becomes smaller, the buckling load decreases less rapidly with respect to the crack length.
Nonami *et al.*[25]	2014	Numerical method (Finite Element Method)	A study on optimisation of the structure of a ship in consideration of the layout of the stiffeners	Stiffened panels	A possible way to reduce ship costs is to optimise the structure with the layout of stiffeners.
Xu *et al.*[21]	2018	Analytical method	Strength of stiffened panels of ship structures	stiffened panels	The load-carrying capacities of stiffened panels with angle and tee bars are comparable, unlike those with flat bars. This difference persists even when the plate slenderness and column slenderness of the panels are very similar.
Sujiatanti *et al.* [32]	2020	Experiment and Numerical method	Cracked thin steel panel under sequential tension and compression	Cracked thin-plates	The presence of a crack in the panel reduces the peak tensile load, and the reduction becomes larger as the crack size increases.
Mantzaroudis and Stamatelos[33]	2020	Analytical method	Local skin buckling of stiffened plates	Stiffened panels with omega stiffeners	The Rayleigh–Ritz method is used to obtain a closed-form expression for the critical compressive load that causes local buckling of omega-stiffened plates with antisymmetric cross-ply and angle-ply laminates.

© Engineered Science Publisher LLC 2024

York[34]	2021	Analytical method	Laminate stiffness tailoring for improved buckling performance	Thin-walled column	One drawback of symmetric designs is that they restrict the design possibilities for common aircraft parts, such as spars, skins, or stiffeners, especially in thin laminates. This is because symmetric designs do not allow Bending–Twisting coupling, which can negatively affect the buckling performance of the structure. Moreover, symmetric designs can never achieve a higher buckling performance than non-symmetric designs.
Oiwa *et al.*[35]	2021	Numerical method (Finite Element Method)	Face sheet buckling for honeycomb sandwich panel	Honeycomb sandwich panels	Two different core models—namely, a detailed core model that accounted for the honeycomb structure and a solid core model that represented the core using solid elements—were utilised to conduct stress and buckling eigenvalue analyses in order to determine the fracture strength of sandwich panels with face sheet buckling.
Peng *et al.*[36]	2021	Experiment	Fatigue response of 2A97 Al-Li stiffened panels	Stiffened panels	When stiffened panels fail in shear, they can exhibit different modes such as global buckling waves, skin cracks, and rivets falling off. The critical buckling load of the stiffened panels depends more on the skin thickness than the ultimate load.
Prato *et al.*[37]	2022	Experiment and Numerical method	Stiffened plates: imperfections and joints	Thin-walled stiffened panels	When structures are reinforced, they can sometimes have small flaws, such as misalignments (when the ends of the components do not line up), joints that are not evenly spaced or positioned on the structure, or joints that are not perpendicular to the connected structures.
Prabowo *et al.* [30]	2022	Numerical method (Finite Element Method)	Buckling of idealised hull structures	Stiffened panels	According to this study, it appears that strengthening the panel through increasing both the thickness of the plate and the longitudinal stringers attached to the specimens results in a higher level of strength. Moreover, altering the plate's thickness had a notable impact on the strength and energy generated during buckling.

components such as plates and columns experience compressive loads that exceed a critical value.[30] At this point, the components deflect out of their original plane, resulting in a rapid increase in out-of-plane deflection. Consequently, the in-plane stiffness decreases, leading to a reduction in the load capacity that can be sustained. Further load increases may result in structural failure due to progressive buckling loads.[38] In 1850, Kirchhoff proposed Kirchhoff's simplest plate theory, also known as the Classical Thin Plate Theory (CPT).[30] This theory makes several assumptions:

1. The deflection of the plate is small, less than the plate's thickness.
2. The centre plane of the plate does not stretch and remains on the neutral surface during bending.
3. The plane sections of the plate can rotate during bending while remaining normal to the neutral surface, without undergoing any distortion. This assumption allows stress and strain to be proportional to the distance from the neutral surface.
4. Shear forces are neglected, and the load is entirely resisted by the bending moment induced in the plate element.
5. The thickness of the plate is not significantly greater than its other dimensions.

When considering the buckling of a thin square plate subjected to biaxial compression loads, the governing equation based on Kirchhoff's theory or Classical Thin Plate Theory (CPT) is given by Equation (1):

$$D\left(\frac{\partial^4 w}{\partial x^4} + 2\frac{\partial^4 w}{\partial x^2 \partial y^2} + \frac{\partial^4 w}{\partial y^4}\right) + N_x \frac{\partial^2 w}{\partial x^2} + N_y \frac{\partial^2 w}{\partial y^2} = 0, \quad (1)$$

where w is the transverse deflection and D is the flexural

© Engineered Science Publisher LLC 2024

rigidity of the slab, as presented in Equation (2).

$$D = \frac{Eh^3}{12(1-v^2)}, \quad (2)$$

where the parameter h represents the plate thickness, E denotes Young's Modulus, and v represents Poisson's ratio. Equations (3) and (4) provide the respective forms for the two boundary conditions and each elastically restrained edge.

$$D\frac{\partial^2 w}{\partial n^2} + Dv\frac{\partial^2 w}{\partial s^2} \mp \frac{K_r^m}{L}\frac{\partial w}{\partial n} = 0, \quad (3)$$

$$N\frac{\partial w}{\partial n} + D\frac{\partial^3 w}{\partial n^3} + (2-v)D\frac{\partial^3 w}{\partial^2 \partial n} \pm K_l^m w = 0, \quad (4)$$

$$N_{cr} = \frac{k_c \pi^2 D}{b^2}, \quad (5)$$

where the normal direction to the edge is denoted by n, and the parallel direction is denoted by s.[39,40] In the case of a square plate with simply supported boundary conditions on all sides (see Fig. 2), the Critical Buckling Load—represented as Equation (5) above—describes the point at which buckling occurs under a compression load. Equation (5) also incorporates the values of n and s.[39,40] The Critical Buckling Load equation depends on various factors, such as the length of the unloaded plate a, the length of the loaded plate b, and the buckling coefficient k_c. Determining D requires Equation (2). Moreover, the value of the buckling coefficient, k_c, is influenced by the ratio of a to b and the type of support on the plate side (*i.e.*, the boundary condition). For a graphical representation of the relationship between the buckling coefficient and the aspect ratio a/b, please refer to Fig. 3.

Figure 4 presents the buckling coefficient for different boundary conditions. Case (A) represents a scenario where all sides are simply supported, while case (B) depicts the clamping of the loaded sides and simple supporting of the unloaded sides. Similarly, case (C) involves the reverse configuration, with loaded sides being simply supported and unloaded sides being clamped. Finally, case (D) demonstrates a situation where all sides are clamped.

Buckling occurs when the applied axial force surpasses a specific critical threshold, as shown in Fig. 2. The computation of the buckling coefficient is performed, and the results are graphically represented in Fig. 3. The transition in buckling mode occurs at the aspect ratio given by $\sqrt{\boldsymbol{m(m+1)}}$, shifting from a mode with $\boldsymbol{m}$ half-waves to a mode with $(\boldsymbol{m+1})$ half-waves. The graph in Fig. 4 illustrates the buckling coefficients in four different scenarios, plotted with respect to the aspect ratio $(\boldsymbol{a/b})$ of the plate. Case (A) exhibits the least buckling strength, indicating that a rectangular plate subjected to uni-axial thrust has the lowest buckling resistance when all four sides are supported. Additionally, it can be observed that the minimum buckling strength under the condition of all sides being simply supported occurs when the aspect ratio is an integer; specifically, when the ratio $\boldsymbol{a/mb}$ is equal to 1.0. When Case (A) and Case (B) are compared, the buckling strength varies at low aspect ratios of the plate but converges as the aspect ratio increases, potentially reaching parity at infinity.

4. Benchmark and validation

4.1 Experimental reference profile

The experimental reference profile utilised in this study is based on the experimental tests conducted by Quinn *et al.*,[41] and involves a stiffened panel structure with stiffener Type I. The specimen comprises three longitudinal stiffeners with dimensions of 590 mm in length, 28 mm in height, and 22.8 mm in thickness, placed parallel to each other on the plate surface. The spacing between the stiffeners is 167 mm. For a visual representation of the reference geometry and dimensions, refer to Fig. 5(a).[41]

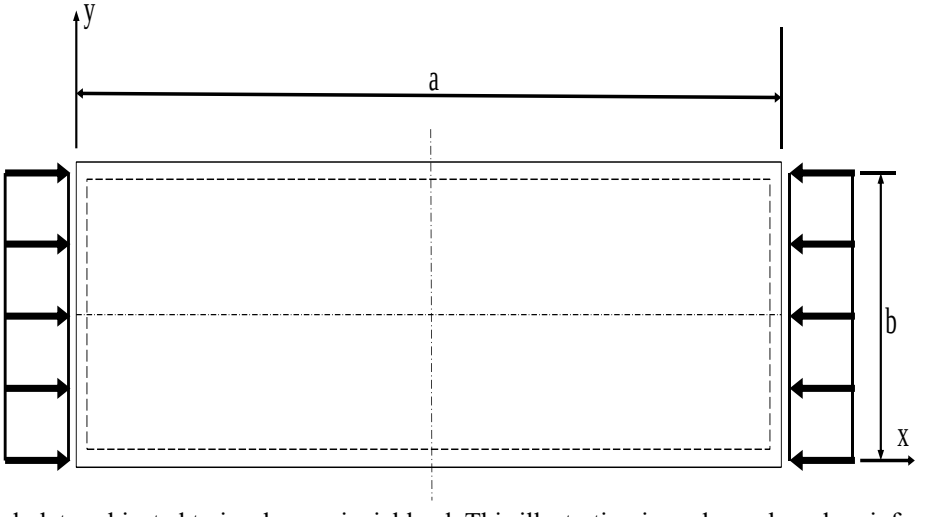

Fig. 2 Simply supported plate subjected to in-plane uniaxial load. This illustration is re-drawn based on information in [39].

 © Engineered Science Publisher LLC 2024

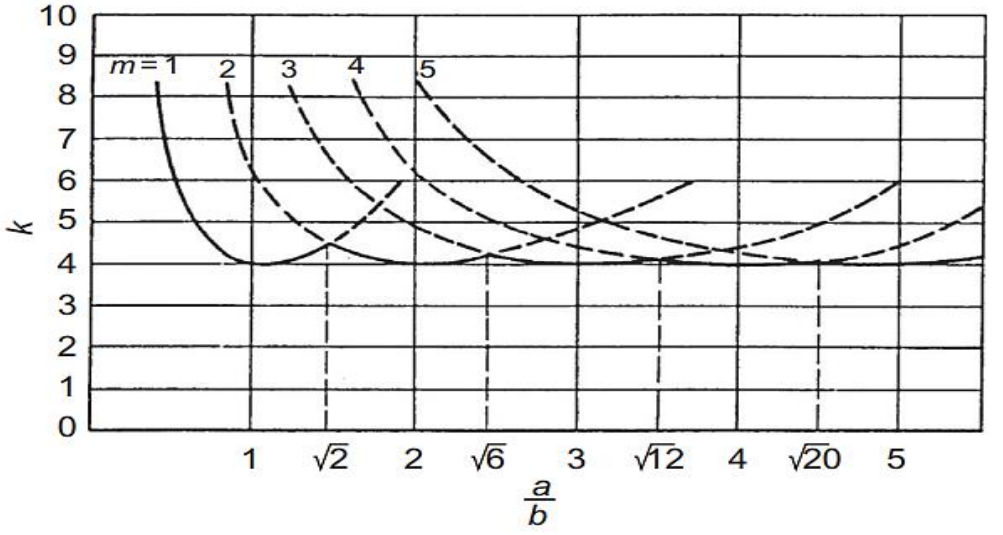

Fig. 3 Buckling coefficient for square plate with varying aspect ratio a/b.[39]

This study refers to the plate structure and stiffener both composed of Aluminium Alloy 2024-T351. However, the specific mechanical properties of this material are not elaborated upon, and additional information regarding these properties can be found in another study conducted by Goldarag *et al*.,[42,43] who also employed the same material. Fig. 5(b) shows the engineering stress–strain graph for both the plate and stiffener materials. Experiments were performed using a hydraulic testing machine with a capacity of 500 kN. A 42 mm thick epoxy-reinforced resin base was positioned at each loading end of the specimen, in order to enforce a clamped boundary condition. Strain gauges were affixed to the.

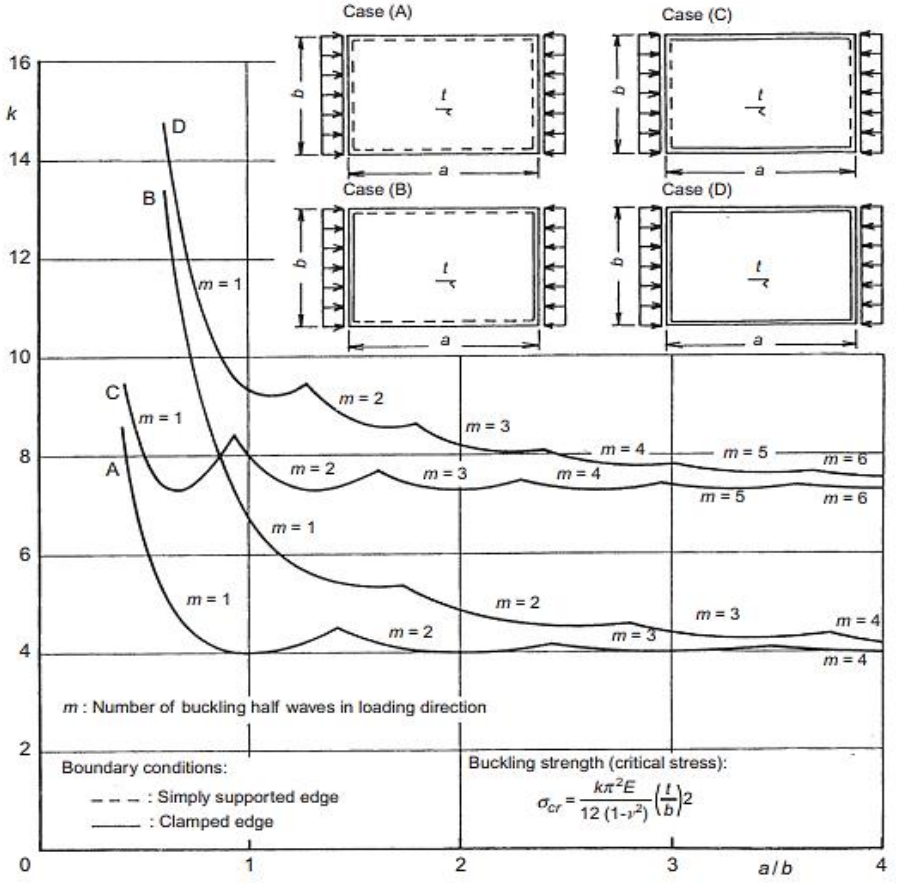

Fig. 4 The buckling coefficient of a rectangular plate under various boundary conditions. Reproduced with the permission from [39], Copyright 2017 Elsevier Ltd.

© Engineered Science Publisher LLC 2024

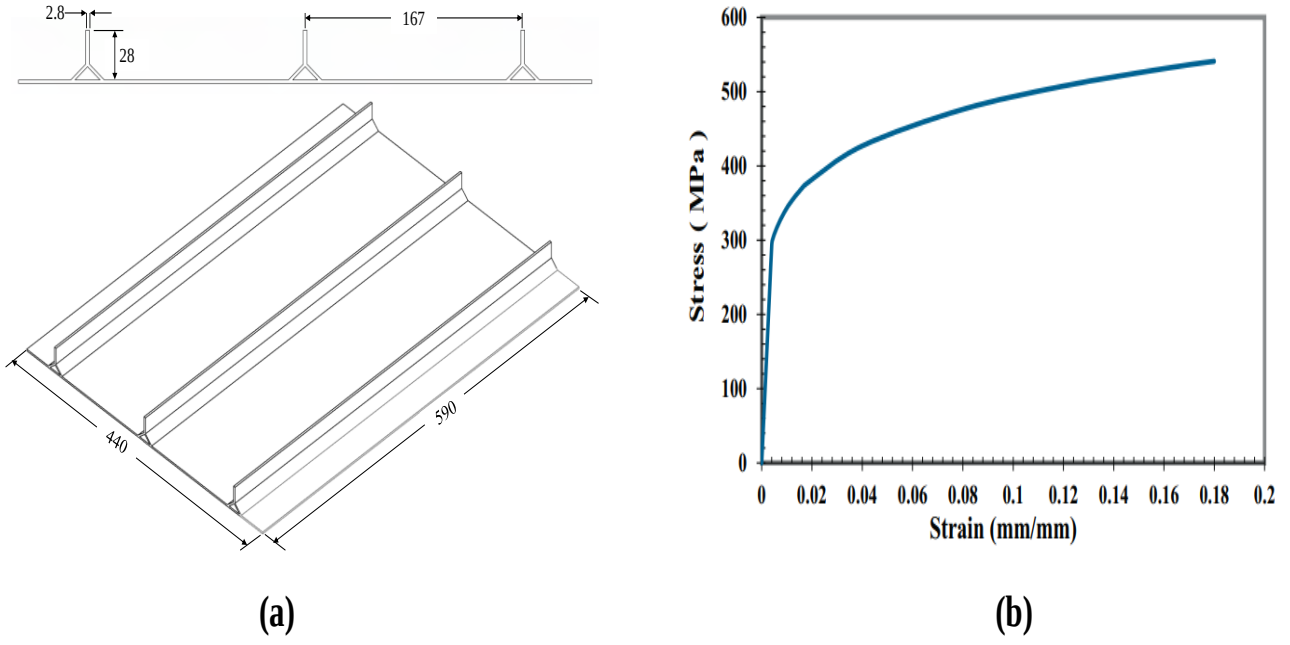

Fig. 5 (a) Geometry and dimensions of stiffened panel structure testing experiment (re-drawn based on [41]). All dimensions are in millimeters (mm); (b) Aluminium Alloy 2024-T351 engineering stress–strain graph [42,43].

specimen during the experimental tests to assess initial plate buckling and post-buckling failure. Furthermore, displacement measurements of the specimen were recorded using two calibrated displacement transducers, each placed on one side of the specimen

4.2 Simulation validation procedure

The validation procedure was carried out using benchmarking studies against experimental test data as a reference, with the aim of reducing the error that occurs in the simulation data such that valid and accurate simulation data are obtained. The validation procedure in this study was carried out through comparing load–displacement graphs, fracture energy values, and deformation contours generated from experimental testing and simulation testing using ANSYS Workbench[44], with minimal disparity compared to the experimental data. The linear analysis of buckling loading has the objective of determining the critical load on the specimen and also the effect of buckling loading on the specimen below the yield point. Meanwhile, the non-linear analysis is intended to observe the effect of the buckling load after passing the yield point and also to determine the ultimate panel collapse load of the specimen. Both analyses are incorporated into the static structural analysis, commencing with the input of material information for the specified model, including the setup of the non-linear isotropic hardening power law for non-linear analysis. Subsequently, the specimen model—representing the shell of the stiffened panel with assigned thickness—is introduced. Setup data for the analysis, such as mesh size connection, boundary conditions, and analysis solution, are then provided, which determine the type of linear or non-linear analysis.

4.3 Experiment versus numerical analysis

The accuracy of simulation testing can be assessed by comparing the obtained force–displacement relationship with that obtained through experimental testing. This evaluation involves visually and numerically comparing the force and displacement data obtained with both methods. Fig. 6 illustrates the load–displacement comparison, while Table 2 provides the corresponding numerical values. Additionally, a mesh convergence analysis is conducted at peak load (Fig. 6 and Table 2), which compares the results obtained when using different mesh sizes (ranging from 10 mm to 50 mm). The error between the numerical and experimental results was calculated for each mesh size. These analyses consistently yielded an error below 10% for all specimens with a deformation limit of 3 mm, indicating a favourable agreement between the numerical and experimental data. Furthermore, the accuracy of the simulation results was evaluated through comparing the deformation contours of the structure with those obtained from experimental tests. Deformation contours depict the distribution of strain and stress on the surface of the structure under loading conditions. Fig. 7 presents a comparison of the deformation contours between experimental and simulation tests. The analysis reveals that

 © Engineered Science Publisher LLC 2024

the base plate experienced higher deformation.

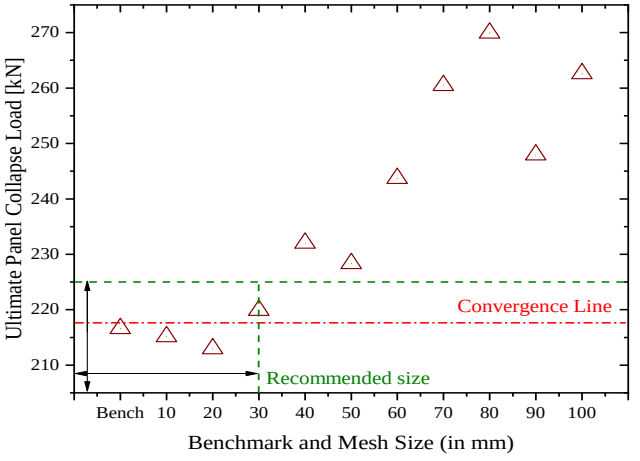

Fig. 6 Load–displacement comparison graph. Benchmark data were taken from the experiment of Quinn *et al.*[41]

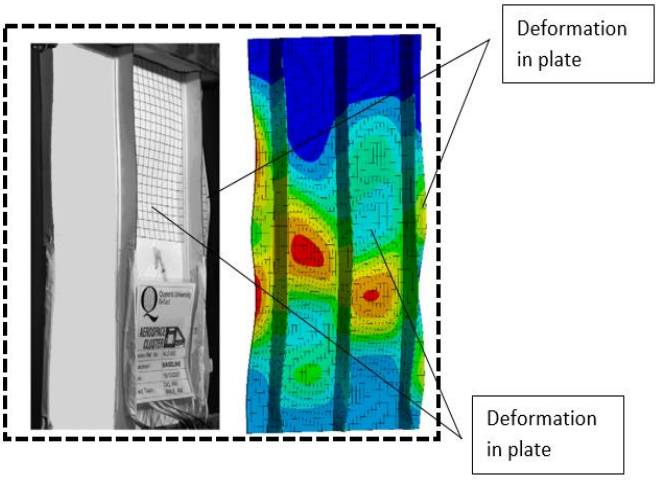

Fig. 7 Comparison between experimental object considered by Quinn *et al.*[41] and the FEs on a stiffened panel considered in this study.

5. Parametric study

The primary objective of this research project is to investigate the performance of stiffened plate structures under buckling load conditions. To achieve this objective, a systematic and rigorous approach was followed, consisting of several stages. The initial stage involved conducting a comprehensive review of the literature to develop a numerical prototype model of the plate structure with an optimal stiffener configuration for resisting buckling loads. This model was then validated and calibrated using both experimental data and analytical solutions. Subsequently, the validated model was utilised to conduct parametric studies and sensitivity analyses, aiming to identify the key factors that significantly influence the buckling load performance. The outcomes of these analyses are thoroughly presented and discussed in this paper. For a visual representation of the research stages, refer to Fig. 8, which depicts the flowchart of the study.

Table 2. Ultimate panel collapse loads and percentage of load difference.

Conducted Research	Mesh Size [mm]	Ultimate Panel Collapse Load [kN]	Load difference percentage [%]
Experimental data [41]	-	216.6	-
Current Study	10	215.14	0.67
	20	212.96	1.68
	30	219.89	1.52
	40	232.03	7.12
	50	228.33	5.42
	60	243.7	12.51
	70	260.45	20.24
	80	269.93	24.62
	90	247.93	14.46
	100	262.6	21.24

5.1 Geometric model

The simulation's structural geometry refers to the specific shape and arrangement of the elements composing the structure being studied. This geometry corresponds exactly to the one employed in the experimental reference, which represents a previous study that involved tests on the same structure within a laboratory environment. The simulation adopted the dimensions of the stiffened panel structure—namely, a length of 590 mm, width of 440 mm, stiffener height of 28 mm, and plate thickness of 2.2 mm—which were derived from the experimental reference and conveniently presented in Table 3. The considered structural geometry consisted of plates and three attached stiffeners, as depicted in Fig. 9, which provides labels for each component. Adjustments to the structural geometry were made by incorporating variations in stiffener type, stiffener spacing, and stiffener configuration.

5.2 Material model

The selection of an appropriate material model is essential in order to accurately represent the structural behaviour of a material under various loading conditions, based on experimental results from a reference source. According to Goldarag *et al.*,[41,42] Aluminium Alloy 2024-T35 is considered a suitable material for this purpose. This alloy possesses specific mechanical properties, as outlined in Table 4, and is commonly applied in aircraft structures, including wings and fuselages. The density of Aluminium Alloy 2024-T35 is 2780 kg/m^3, with a Young's modulus of 73.4 GPa, a yield stress of 315 MPa, a tensile strength of 550 MPa, a Poisson's ratio of 0.33, an exponent of 0.406, and a failure strain of 0.18.

© Engineered Science Publisher LLC 2024

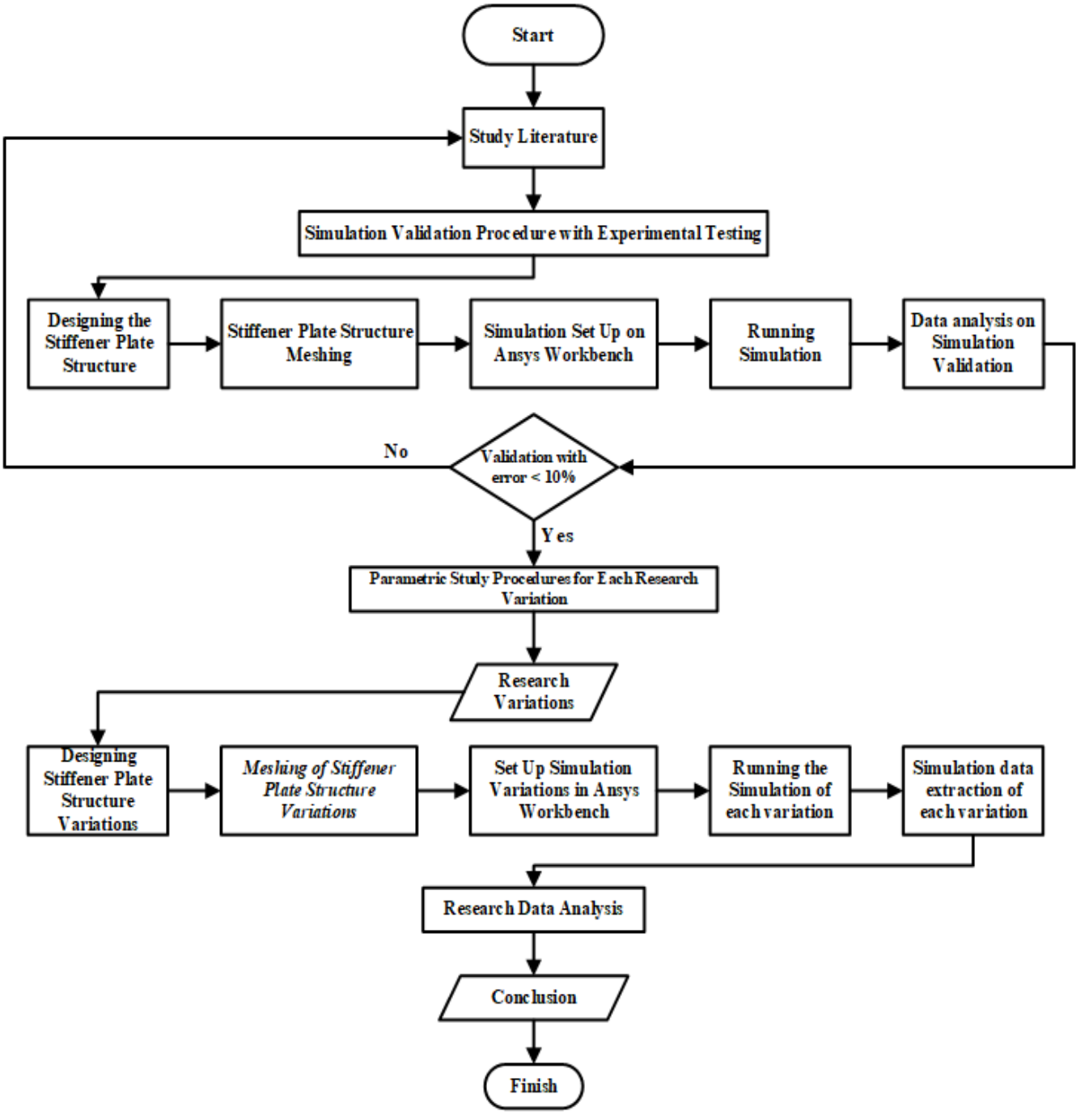

Fig. 8 Flowchart of the benchmarking and parametric study for the designed FE procedure.[45-52]

Table 3. Dimension of stiffened panel structure.

Cross-Section s	Cross-section view	Dimension (mm)
Transverse cross-section	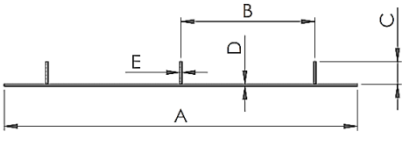	A = 440 D = 2.2 B = 167 E = 2.8 C = 28
Longitudinal cross-section	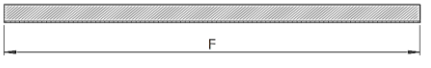	F = 590

© Engineered Science Publisher LLC 2024

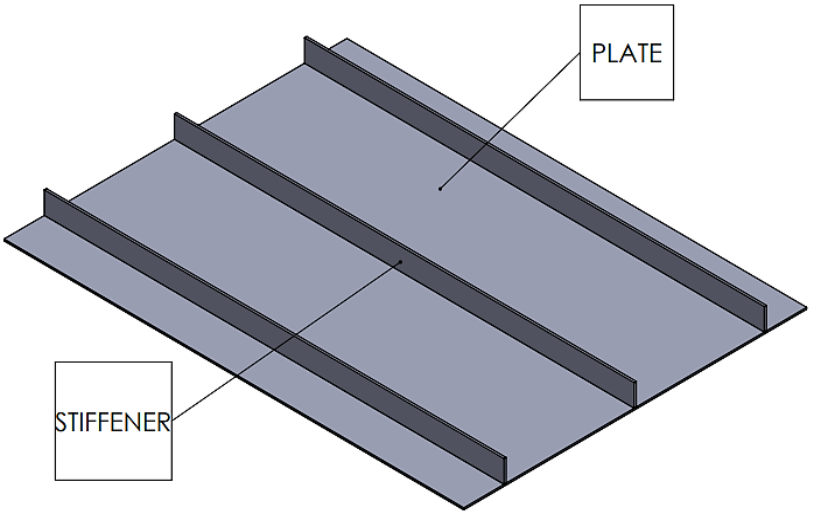

Fig. 9 Geometry of the stiffened panel structure.

Table 4. Mechanical properties of stiffened panel material based on information in [41,42].

Property	Value
Density (kg/m^3)	2780
Young's modulus (GPa)	73.4
Yield strength (MPa)	315
Tensile strength (MPa)	550
Poisson's ratio (-)	0.33
Exponent (-)	0.406
Failure strain (-)	0.18

5.3 Loading scheme and boundary conditions

This study presents two types of buckling simulation schemes: linear and non-linear analyses. Each analysis type employs distinct schemes and boundary conditions. The linear buckling analysis assumes that the structure behaves linearly until it reaches a critical load, which induces instability. The boundary conditions for this analysis involve simple support on all sides. Specifically, the displacements on the top, bottom, right, and left sides are unrestricted in the x- and y-axes, while being fixed in the z-axis. Rotation on the top and bottom sides is fixed along the y-axis while being unrestricted along the x- and z-axes. Rotation on the left and right sides is fixed along the y-axis and unrestricted along the z-axis. Additionally, an opposing force of 10 N/m is applied to the top and bottom sides. In the centre of the plate, the displacement is unrestricted along the z-axis and fixed in the x- and y-axes. Further information is provided in Fig. 10. On the other hand, non-linear buckling analysis considers the geometric non-linearity of the structure caused by significant deformations. It follows the equilibrium path of the structure beyond the critical load, until it reaches a limit point or a bifurcation point. This analysis requires a distinct scheme which is capable of handling non-linear equations of motion and a different set of boundary conditions to simulate realistic loading scenarios.

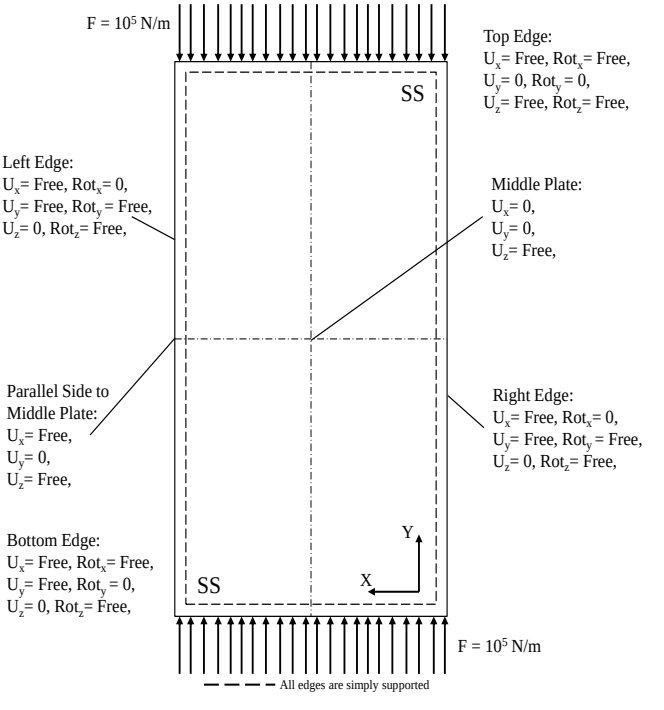

Fig. 10 Boundary conditions used in linear buckling analysis. This illustration is re-drawn based on information in [41].

The boundary conditions for the reference validation model in the non-linear analysis were as follows: the top side of the specimen is clamped, allowing displacement only along the x-axis and fixed in the y- and z-axes. The bottom side is also clamped but allows displacement along the x- and y-axes, while being fixed in the z-axis. Rotation is unrestricted in the x- and y-axes and fixed in the z-axis for both the top and

© Engineered Science Publisher LLC 2024

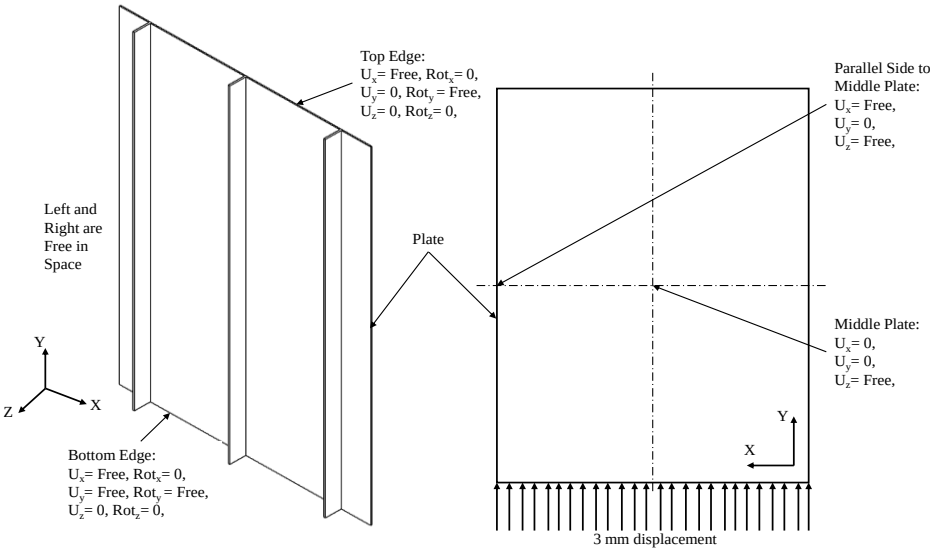

Fig. 11 Boundary conditions used in benchmarking non-linear buckling analysis. This illustration is re-drawn based on information in [41].

bottom sides. A displacement of 3 mm parallel to the y-axis is applied to the bottom side. The right and left sides are left unfixed. At the centre, displacement is allowed only on the z-axis, while the x- and y-axes are fixed. For the study involving various stiffener scenarios, the boundary conditions required a displacement change of 25 mm. This displacement change causes the simulated stiffened panel structure to reach the desired buckling collapse behaviour, corresponding to the failure point. Detailed illustrations of the non-linear boundary conditions are shown in Figs. 11 and 12.

5.4 Scenario variation

This study examines various scenarios based on variations that impact the structural behaviour of the model. These variations can be categorised into two groups: physical parameter variations and numerical parameter variations. Physical parameter variations involve changes in the type, spacing, and configuration of the stiffeners attached to the model, while numerical parameter variations involve modifications in the mesh size used for discretising the model during numerical analysis. The volume and density of the designed stiffeners were set as dependent variables. The objective of varying the stiffener type in this study is to investigate the influence of different stiffener types on the performance of stiffened panels under loads. Four stiffener types—including type I, type L, type T, and type Y (Fig. 13)-were considered. The volume of each stiffener type was kept constant at 8.64×10^6 mm^3. Tables 5 and 6 provide the dimensions for the various stiffener types.

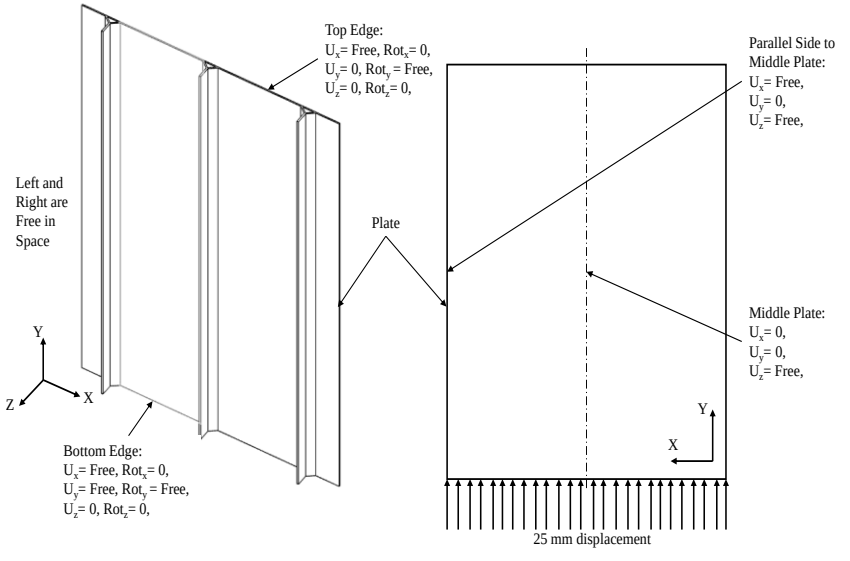

Fig. 12 Boundary conditions used in benchmarking non-linear buckling analysis. This illustration is re-drawn based on information in [41].

 © Engineered Science Publisher LLC 2024

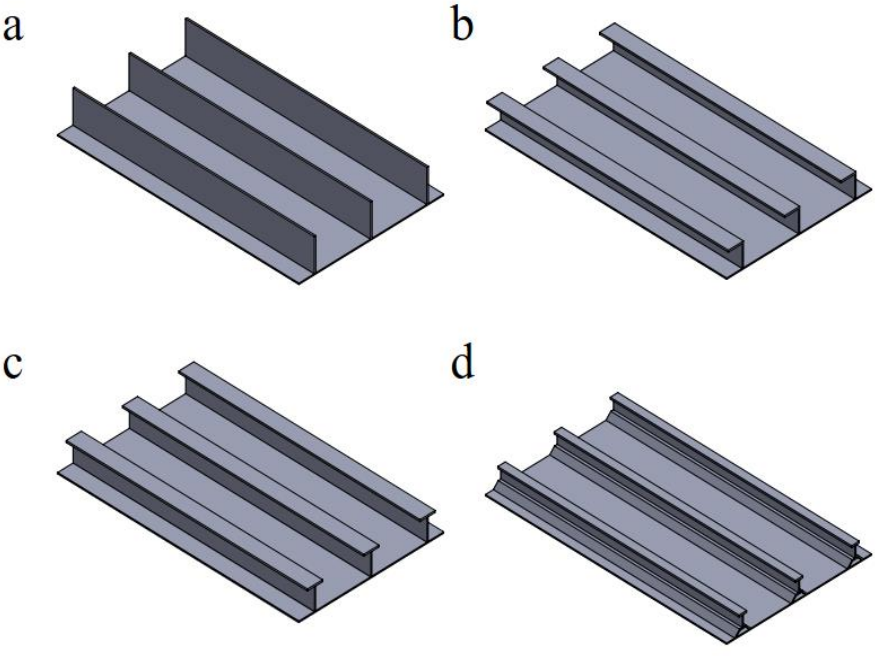

Fig. 13 Stiffener type geometry: (a) Type-I; (b) Type-L; (c) Type-T; and (d) Type-Y.

Table 5. Codes of stiffener type variations.

Stiffener Type	Code
I	Type-I
L	Type-L
T	Type-T
Y	Type-Y

This study examines the effect of stiffener spacing on the buckling behaviour of a stiffened panel structure under axial load, involving four different stiffener spacings: one with a spacing of 360 mm, two with a spacing of 180 mm, and three with a spacing of 80 mm (using stiffener type Y as a model, as depicted in Fig. 14). Decreasing the spacing between stiffeners results in an increased number of stiffeners within the structure. The specific variation codes and dimensions of the stiffener spacing variations can be found in Tables 7 and 8, respectively.

Table 7. Codes for differently spaced stiffeners.

Distance (mm)	Code
360-360	Dist-1
180-360-180	Dist-2
80-280-280-80	Dist-3

Table 6. Dimensions of various stiffener types.

Type	Geometry	Dimension (mm)	Type	Geometry	Dimension (mm)
I	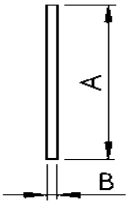	A = 150 B = 6.5	T	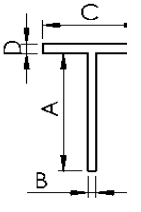	A = 100 B = 6 C = 75 D = 8
L	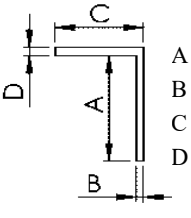	A = 100 B = 6 C = 75 D = 8	Y	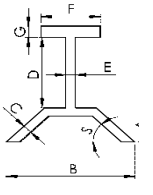	A = 24.2 B = 80.9 C = 6 D = 50 E = 6 F = 37.5 G = 8 S = 45°

© Engineered Science Publisher LLC 2024

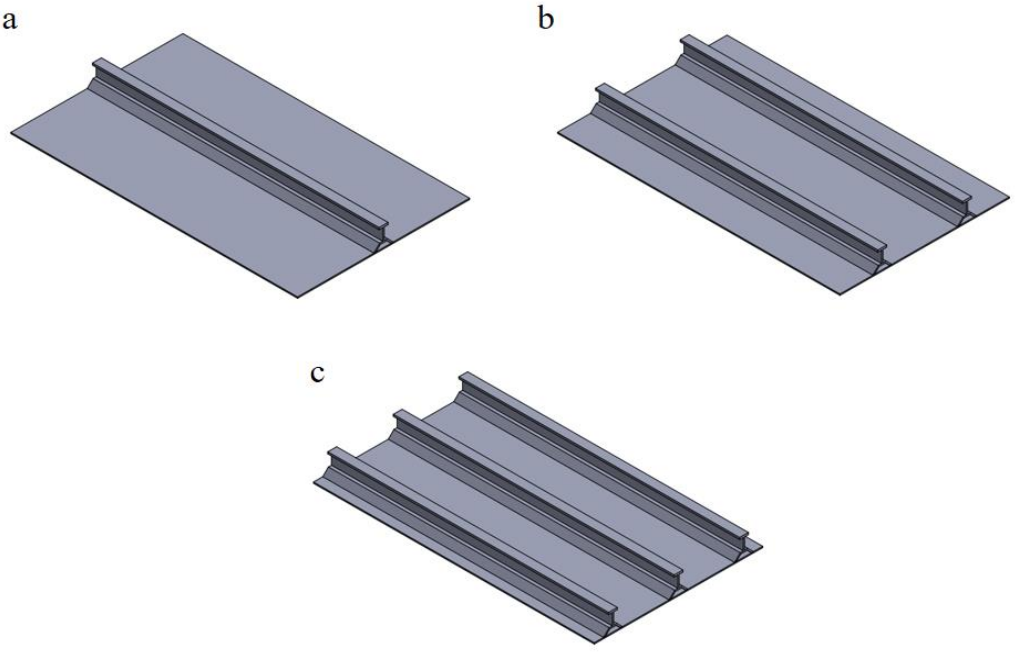

Fig. 14 Geometric models of various stiffener spacings: (a) Dist-1; (b) Dist-2; and (c) Dist-3.

Table 8. Variations of stiffener spacings.

Variation of spacing of stiffener	Geometry	Dimension (mm)
Dist-1 (360 mm -360 mm)	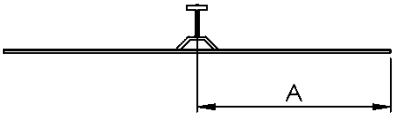	A = 360
Dist-2 (180 mm - 360 mm- 180 mm)	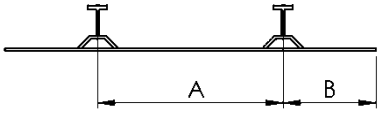	A = 360 B = 180
Dist-3 (80 mm-280 mm- 280 mm-80 mm)	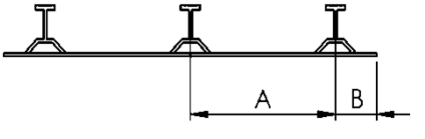	A = 280 B = 80

The effects of stiffener configuration on the structural response under impact loads were examined. Six different stiffener configurations were considered: Configuration 1 (1-Transverse and 1-Longitudinal), configuration 2 (1-Transverse and 2-Longitudinal), configuration 3 (2-Transverse and 1-Longitudinal), configuration 4 (2-Transverse and 2-Longitudinal), configuration 5 (3-Transverse and 1-Longitudinal), and configuration 6 (3-Transverse and 2-Longitudinal). This investigation focused specifically on the Y stiffener type. The code and dimension tables for the stiffener configuration variations are provided in Tables 9 and 10, respectively. For a visual representation, the geometry of the stiffener configuration variation is presented in Fig. 15.

Table 9. Codes for various stiffener configurations.

Stiffener Configuration	Code
1-Transversal; 1-Longitudial	Config-1
1-Transversal; 2-Longitudial	Config-2
2-Transversal; 1-Longitudial	Config-3
2-Transversal; 2-Longitudial	Config-4
3-Transversal; 1-Longitudial	Config-5
3-Transversal; 2-Longitudial	Config-6

© Engineered Science Publisher LLC 2024

Table 10. Variations of stiffener configurations.

Variation of stiffener configurations	Geometry	Dimension (mm)
Config-1	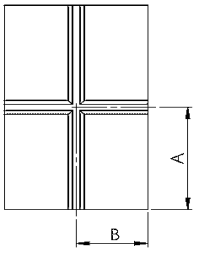	A = 600 B = 360
Config-2	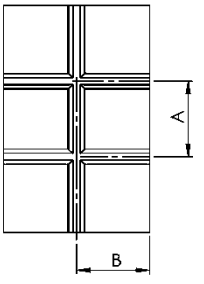	A = 400 B = 360
Config-3	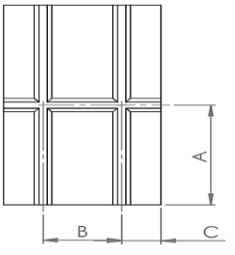	A = 600 B = 360 C = 180
Config-4	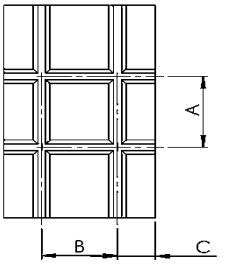	A = 400 B = 360 C = 180
Config-5	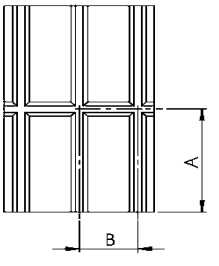	A = 600 B = 280
Config-6	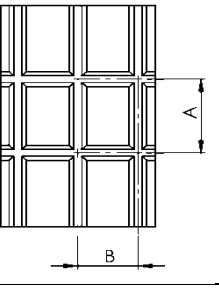	A = 400 B = 280

© Engineered Science Publisher LLC 2024

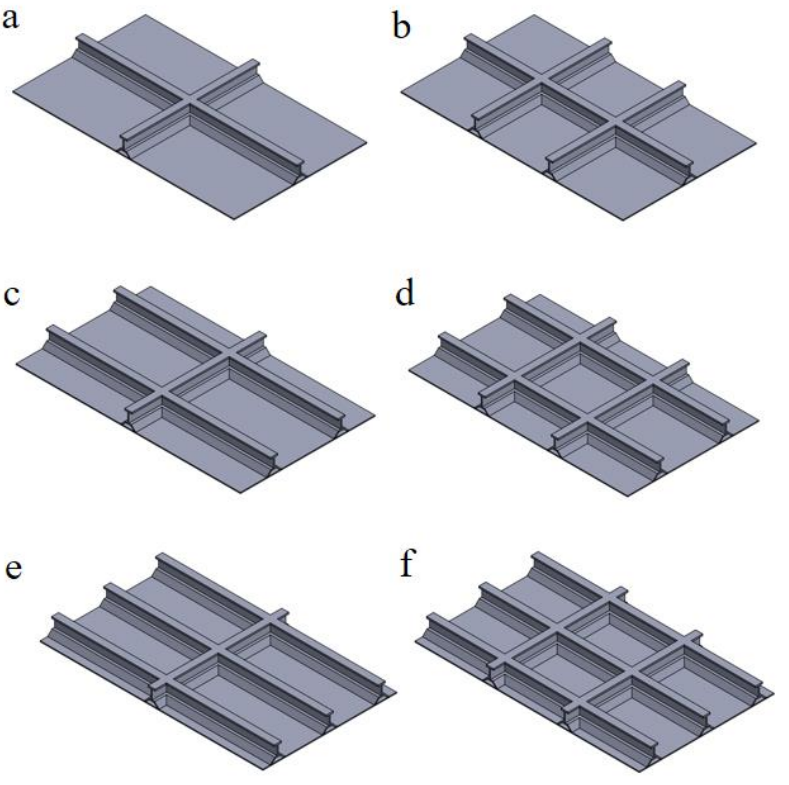

Fig. 15 Geometric models of stiffener configurations: (a) Config-1; (b) Config-2; (c) Config-3; (d) Config-4; (e) Config 5; and (f) Config-6.

The impact of mesh size on the accuracy and quality of simulation results obtained through the finite element method was also assessed. Specifically, we explored the influence of various mesh sizes (ranging from 10 mm to 100 mm) while maintaining a constant geometry for the structure under investigation. The chosen structure's geometry was based on the previously described simulation validation structure. Table 11 provides details on the codes for geometric variations implemented with different mesh sizes.

Table 11. Codes for variation of mesh size.

Mesh Size (mm)	Code
10	Mesh-10
20	Mesh-20
30	Mesh-30
40	Mesh-40
50	Mesh-50
60	Mesh-60
70	Mesh-70
80	Mesh-80
90	Mesh-90
100	Mesh-100

6. Comparison of results under stiffener type variations

The used stiffened panel structures had four different stiffener types; namely, I type, L type, T type, and Y type. Each stiffener type had the same cross-sectional area (equal to 180,000 mm^2), such that each stiffener type had a controlled volume. Analysis of the buckling collapse behaviour can be initially assessed according to the critical buckling load value in the linear analysis; then, in the non-linear analysis, through the ultimate panel collapse load value in the load-displacement graph and the total energy generated in the energy-displacement graph.

6.1 Linear analysis

The results of the linear analysis considering the stiffened panel structures with different stiffener types are presented in this section. The critical buckling load is an important parameter that indicates the structural stability of a panel under compressive loading. Table 11 summarises the values of the critical buckling load for each type of stiffener, while Fig. 16 shows a graphical comparison of these values. As can be seen from Table 12, the stiffened panel with type Y stiffeners had the highest critical buckling load value (of 1,400,000 N/m), which was significantly higher than those of the other types. The second highest value was obtained by type T stiffeners (with 895,370 N/m), followed by type I stiffeners (with 721,380 N/m). The lowest value was found for type L stiffeners, at 677,070 N/m, which is almost half of the value for type Y stiffeners.

 © Engineered Science Publisher LLC 2024

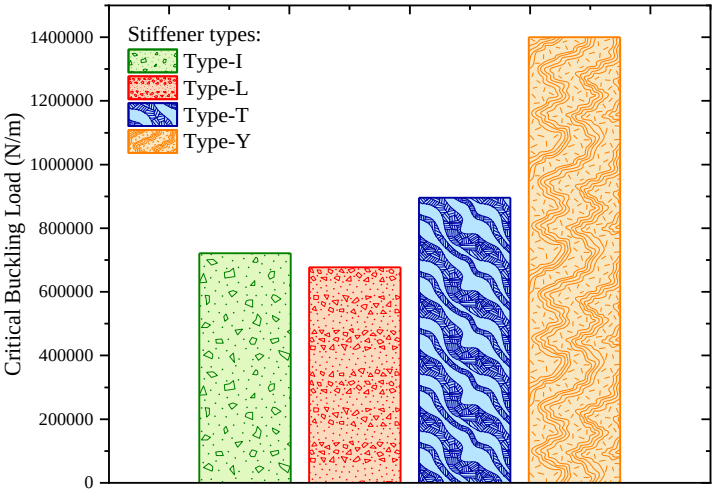

Fig. 16 Comparison of critical buckling load values under stiffener type variations.

Table 12. Effect of variation in stiffener type on critical buckling load.

Specimen	Critical Load (N/m)
Type-I	721,380
Type-L	677,070
Type-T	895,370
Type-Y	1,400,000

In Fig. 16, a diagram comparing the critical buckling load values for each stiffener type variation is presented, which emphasises the significant difference in the critical buckling load value of the stiffened panel structure when using the Y type stiffener compared to the other three stiffener types. The diagram shows that the configuration variation of the stiffener geometry at the same stiffener volume is quite influential on the critical buckling load value of the stiffened panel structure. In the linear analysis, to determine the critical buckling load, the eigenvalue buckling solution method was also applied, such that the contours of each mode of eigenvalue buckling were obtained, which allows for determination of the critical buckling load value based on the applied load. The contours of the first mode of eigenvalue buckling in stiffened panels with various stiffener types are shown in Fig. 17, from which it can be seen that local buckling occurred in the stiffened panel structure precisely on the plate. The Y stiffener type variation showed more buckling waveform formations at the same length and width ratio as all specimens, increasing the buckling coefficient in a manner proportional to the critical buckling load. This was followed by the variation under stiffener type T, then with the variation of stiffener types L and I, which had almost similar buckling waveforms; however, in the variation with stiffener type I, local buckling can be observed in the stiffener.

6.2 Non-linear analysis

Non-linear analysis of the stiffened panel structures with different types of stiffeners was performed, in order to investigate their effects on the structural behaviour. The ultimate panel collapse load, which indicates the maximum load that the panel can withstand before failure, was obtained for each case, as plotted in Fig. 18(a). The total energy generated by the panel during the loading process, which reflects the amount of work done by the applied load and the dissipated energy due to plastic deformation and damage, was also calculated and is shown in Fig. 18(b). The values for all parameters used in the analysis, such as the material properties, the geometry, and the boundary conditions, are presented in Table 13 for reference.

Table 13. Ultimate panel collapse load and total energy.

Specimen	Ultimate Panel Collapse Load (kN)	Energy (kJ)
Type-I	1713.3	37.8
Type-L	2239.5	49.2
Type-T	2408.6	51.9
Type-Y	2973.2	61.6

The buckling collapse behaviour performance of stiffened panels with variation of stiffener type is shown in Figs. 18(a) and (b). The load–displacement graph in Fig. 18(a) illustrates that the displacement along the y-axis changes by 25 mm and how this affects the buckling load that is required to achieve a certain level of deformation, which reveals that, among the different types of stiffeners, the type Y variation had the highest buckling performance, as indicated by its peak point. The L- and T-type stiffeners had similar performances, but the T-type variation had a slightly higher peak point than the L-

© Engineered Science Publisher LLC 2024

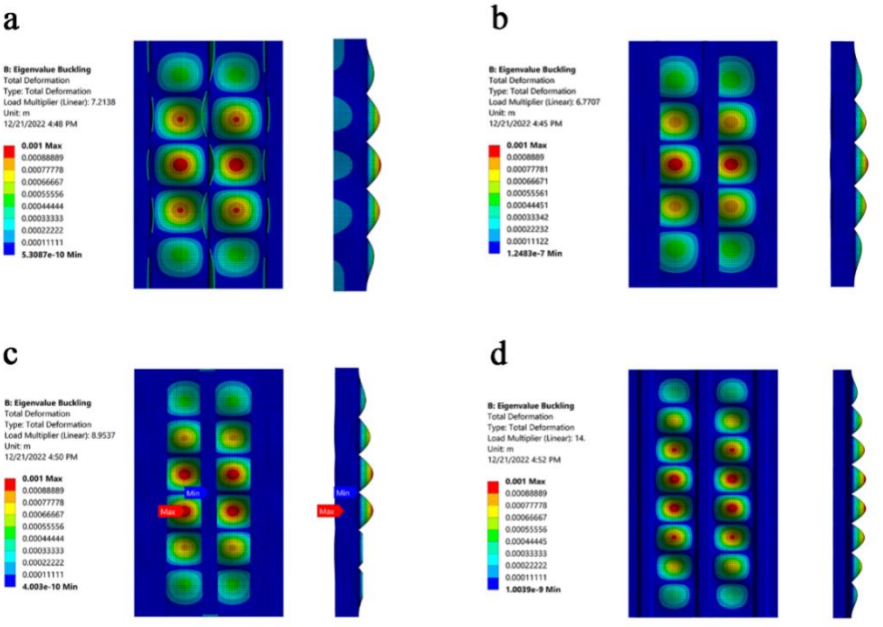

Fig. 17 Buckling Eigenvalue Mode Contour: (a) Type-I; (b) Type-L; (c) Type-T; and (d) Type-Y.

type. The lowest buckling performance was observed with the I-type stiffener. The total energy created at the time of buckling performance is shown in Fig. 18(b). This total energy ends when the displacement reaches a value of 25 mm. The energy-displacement graph shows a trend similar to the that observed in the load-displacement graph, where the Y-type stiffener had the highest total energy, followed by the T-, L-, and I-type stiffeners, respectively.

Based on the data in Table 12, the value of the ultimate panel collapse load had the highest value for the Y-type stiffener, which was equal to 2973.2 kN. This value is significantly higher than those of the other types of stiffeners; namely, T-, L-, and I-type stiffeners presented values of 2408.6 kN, 2239.5 kN, and 1713.3 kN, respectively. This means that the Y-type stiffener increases the ultimate panel collapse load value by 73.3 %, 32.7 %, and 23.4 %, when compared to the I-, L-, and T-type stiffeners, respectively.

The data in Table 12 reveal the amount of total energy produced under the different variations of stiffeners. Among the four types of stiffeners, the Y-type stiffener variation had the highest total energy value, equal to 61.6 kJ. The next highest value was 51.9 kJ, which belonged to the T-type stiffener, followed by the L-type stiffener variation with 49.2 kJ. The lowest value of total energy is 37.8 kN, observed for the I-type stiffener variation. This implies that the Y-type stiffener variation can increase the energy value by 62.9 %

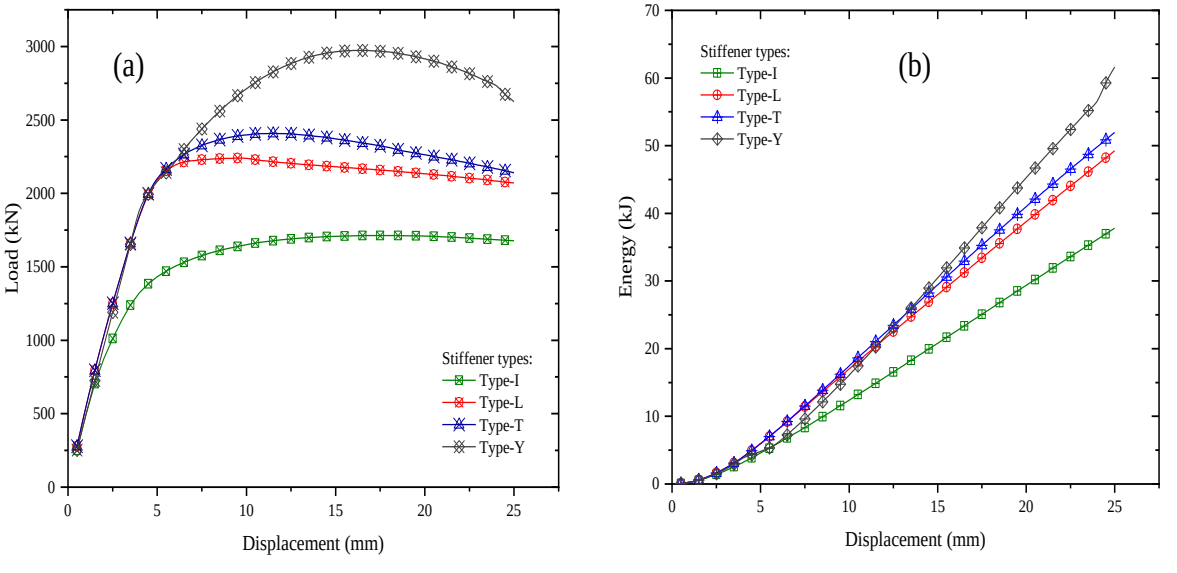

Fig. 18 Graphs of variation in stiffener type: (a) Load-displacement; and (b) energy-displacement.

© Engineered Science Publisher LLC 2024

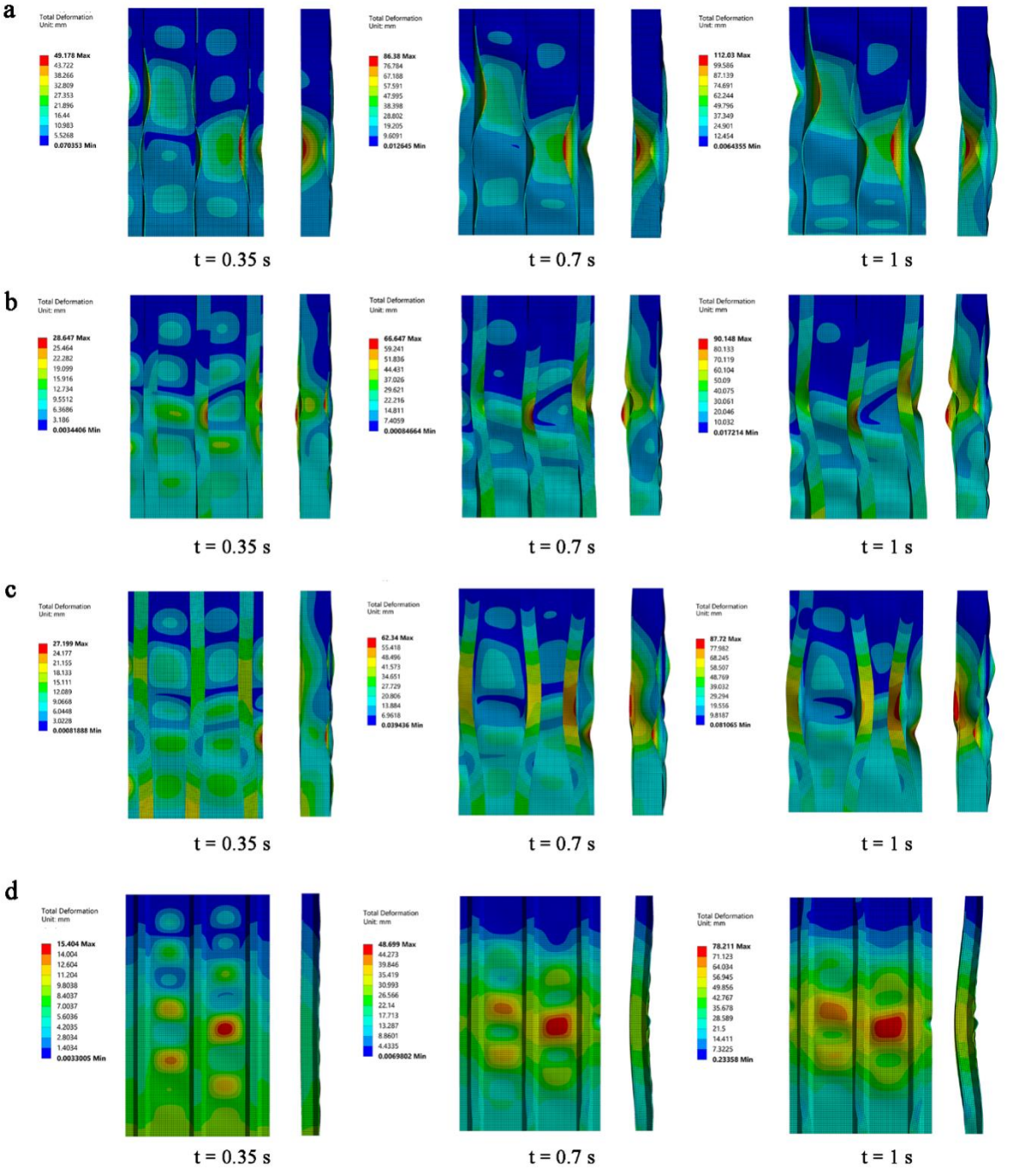

Fig. 19 Equivalent deformation contours on the specimen: (a) Type-I; (b) Type-L; (c) Type-T; and (d) Type-Y.

compared to the I-type stiffener, 25.2 % compared to the L-type stiffener, and 18.6 % compared to the T-type stiffener.

The total energy and ultimate panel collapse load values under the four stiffener types shown in Figs. 18(a) and (b), along with Table 12, indicate significant differences between each variation, especially for the type-Y stiffener variation, which obtained the highest ultimate panel collapse load and total energy values, when compared with the other three variations. In the graphs in Fig. 18, the buckling performance also showed an upward trend with the lowest order in the variation of stiffener type I, followed by types L, T, and Y (the highest). This indicates that, at a controlled volume, the configuration of the stiffener geometry has a very important influence on the buckling performance of stiffened panels, where stiffened panels with type Y variations have the best buckling collapse behaviour performance, compared to other variations. In the non-linear analysis, the equivalent contours of each stiffened panel with different stiffener types were also obtained. The contours displayed in this analysis are the contours equivalent to the deformation and stress during

© Engineered Science Publisher LLC 2024

buckling performance assessment. The variation of stiffener type also affected the distribution of deformation and stress in the stiffened panels. Each stiffened panel was analysed at the three time steps of 0.35 s, 7 s, and 1 s. The equivalent deformation and stress contours are shown in Figs. 19 and 20, respectively.

In Fig. 19, the equivalent deformation contours of the stiffened panels of various variations are shown. Specifically, in Fig. 19(a), for the I-type stiffener, at the beginning of the buckling performance, it can be seen that deformation occurs precisely in the stiffener that experiences local buckling at a time step of 0.35 s. Then, at 0.7 s, the distribution of deformation in the stiffener and plate can be seen. Finally, the contour shows deformation centred in the middle of the stiffened panels—more precisely, on the stiffener and the side of the plate parallel to the centre point—with the maximum deformation reaching 122 mm; this being the largest deformation produced, when compared to the other three variations.

Then, for L- and T-type stiffener variations, as shown in Figs. 19(b) and (c), the buckling performance was similar. At the beginning, there was no apparent deformation change in the stiffened panel; however, at 0.7 s, deformation changes and their distribution contours are visible. Then, in the

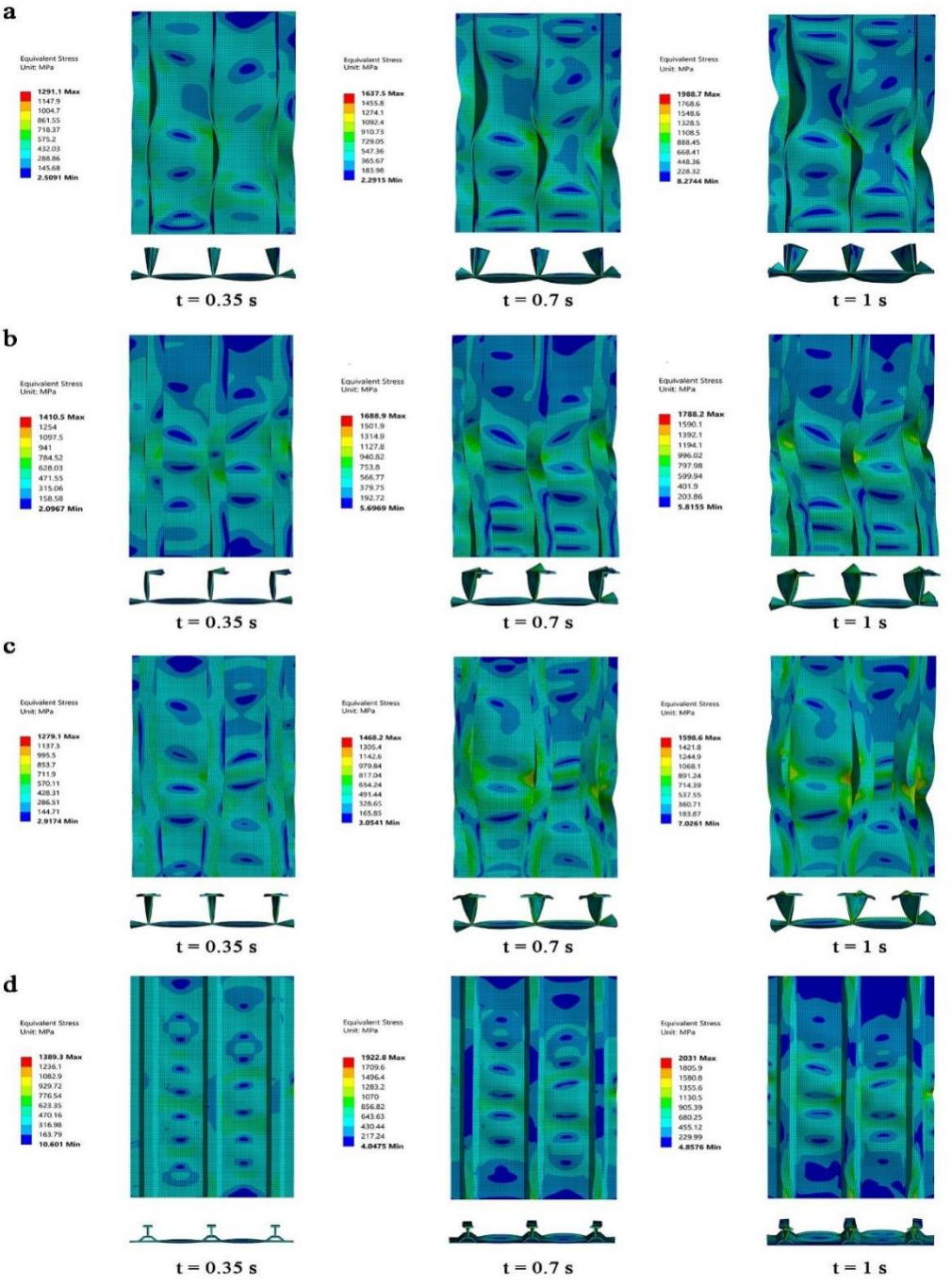

Fig. 20 Equivalent stress contours on the specimen: (a) Type-I; (b) Type-L; (c) Type-T; and (d) Type-Y.

© Engineered Science Publisher LLC 2024

end, the contour shows deformation centred on the middle stiffener, which experiences local buckling, and the side of the plate that is parallel to the centre point of the plate. The L- and T-type stiffener variations obtained maximum deformation values of 90.14 mm and 87.72 mm, respectively.

For the final variation-that is, the Y-type stiffener shown in Fig. 19 (d)-there was still no visible change in deformation at the beginning of the buckling performance; however, at 0.7 s, an even and centralised distribution of deformation is observed due to global buckling. Then, at the end, the stiffened panel deformation is centred in the middle of the stiffened panel, with a maximum deformation reaching 78.21 mm; which is the smallest when compared to the other three variations. This proves the previous statement that the stiffened panel with Y-type stiffener variation has the best buckling collapse behaviour performance, with minimal deformation produced.

The equivalent stress contours for the different types of stiffeners used in the stiffened panels are presented in Fig. 20, which shows the distribution of stresses generated in the panels at three different time steps. In Fig. 20(a), the stress contours for the I-type stiffener variation are displayed, from which it can be observed that, at the initial time step of 0.35 s, the stress concentration is mainly located on the stiffener and the plate is not significantly affected. However, as the time progresses to 0.7 s, the stress distribution spreads to the plate and becomes more pronounced in the middle part of the stiffened panel, where the deformation is higher. At the final time step of 1.05 s, the stress reaches its maximum value of 1988.2 MPa at the centre of the stiffened panel, indicating a large deformation and possible failure of the panel.

As shown in Figs. 20(b) and (c), the buckling performance and stress distribution of the L- and T-type stiffeners were similar. In the initial stage of the simulation, there was no noticeable concentration of stress on the two panels that are reinforced with these stiffeners. However, at 0.7 s, a significant stress concentration emerges in the middle region of the two stiffened panels, accompanied by a visible deformation. In contrast, the T-type stiffener variation exhibited a lower stress concentration on the upper and lower edges of the stiffener, which indicates a better load transfer capability. At the final stage of the buckling performance test, the stress concentration and deformation were both localised at the centres of the two stiffened panels, with the maximum stresses reaching 1788.2 MPa and 1598.6 MPa, respectively.

In the last variation-namely, the Y-type stiffener variation (Fig. 20(d))-the stress distribution on the stiffener was not yet apparent or concentrated on any specific parts at the initial stage of the buckling performance. However, at 0.7 s, the stress distribution becomes uniform throughout the section due to the occurrence of global buckling in the stiffened panel. This global buckling phenomenon affects the entire stiffened panel structure and causes the maximum stress to be located in the middle of the panel. The maximum stress value in this variation is 2031 MPa, which is higher than the other three variations. As a result of having a more even and better stress distribution, compared to the other three stiffener type variations, the stiffened panel with Y-type stiffener exhibited the best buckling collapse behaviour performance among all the variations, as stated earlier.

7. Comparison of results on stiffener distance variations

The spacing and number of stiffeners used in the stiffened panel structure vary depending on the design parameters. The number of stiffeners ranged from 1 to 3, and the spacing between different stiffeners was either 360 mm or 280 mm. The stiffened panels analysed used Y-type stiffeners, being the stiffener type with the best buckling collapse behaviour performance, as determined in the previous analysis. The buckling collapse behaviour analysis was assessed starting from the critical buckling load value in the linear analysis, then through the non-linear analysis regarding the ultimate panel collapse load according to the load-displacement graph and the total energy generated in the energy-displacement graph.

7.1 Linear analysis

The linear analysis of the stiffened panel structure with variations in stiffener spacing revealed how the value of the critical buckling load changes depending on the number and spacing of the stiffeners. The results are presented in Table 14 and illustrated in the diagram in Fig. 21. As can be seen from Table 14, the stiffened panel with three stiffeners and a distance of 280 mm between stiffeners (Dist-3) exhibited the highest critical buckling load value of 1,400,000 N/m, which is almost twice as high as the value for the stiffened panel with two stiffeners and a distance of 360 mm between stiffeners (Dist-2; 729,950 N/m). The lowest value of critical buckling load was obtained for the stiffened panel with one stiffener and a distance of 360 mm to the side, which was only 450,280 N/m. This indicates that increasing the number and decreasing the distance of stiffeners can significantly enhance the buckling resistance of the stiffened panel structure. From the data in Table 14, it can be interpreted that the addition of stiffeners to the plate increases the critical load by 62.11 %, comparing the Dist-1 and Dist-2 specimens. Then, the addition of stiffeners and reducing the distance between stiffeners increases the Critical Load by 91.79 %, comparing between Specimens Dist-2 and Dist-3.

© Engineered Science Publisher LLC 2024

Table 14. Effect of stiffener spacing variation on critical buckling load.

Specimen	Critical Load (N/m)
Dist-1	450,280
Dist-2	729,950
Dist-3	1,400,000

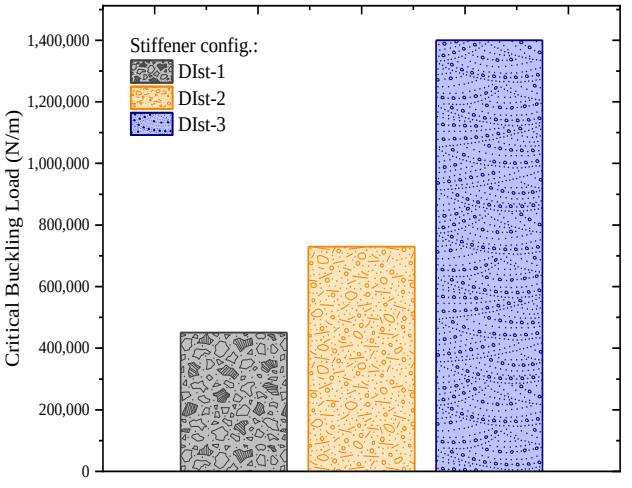

Fig. 21 Comparison of critical buckling load values on variations in the number and spacing of stiffeners.

In Fig. 21, a diagram showing the buckling load under each variation in the number and distance between stiffeners is presented, which indicates a considerable difference in the critical buckling load value when adding stiffeners (Dist-1 vs. Dist-2). Furthermore, adding stiffeners and reducing the distance between stiffeners also increases the critical buckling load value significantly (Dist-2 vs. Dist-3). The diagram shows that the variation in the number and distance between stiffeners on the same plate significantly affects the critical buckling load value of the stiffened panel structure. In the linear analysis, to obtain the buckling load, the eigenvalue buckling solution method was also applied to obtain the contours of each mode of eigenvalue buckling, which determines the value of the critical buckling load based on the applied load. The contours of the first mode of eigenvalue buckling of stiffened panels with variations in the number and spacing of stiffeners are shown in Fig. 22.

Figure 22 shows the contour of the first mode of eigenvalue buckling, from which it can be seen that local buckling occurred in the stiffened panel structure precisely on the plate. In terms of the variation in the number and configuration of stiffeners, Dist-3 showed more buckling waveform formation on the plate with the same length and width ratio as all specimens, increasing the buckling coefficient, which is proportional to the magnitude of the critical buckling load. This was followed by Dist-2, and then Dist-1.

7.2 Non-linear analysis

Non-linear analysis of the stiffened panel structures with variations in the number and distance between stiffeners was performed to investigate the ultimate strength and buckling collapse behaviour of the panels under combined in-plane

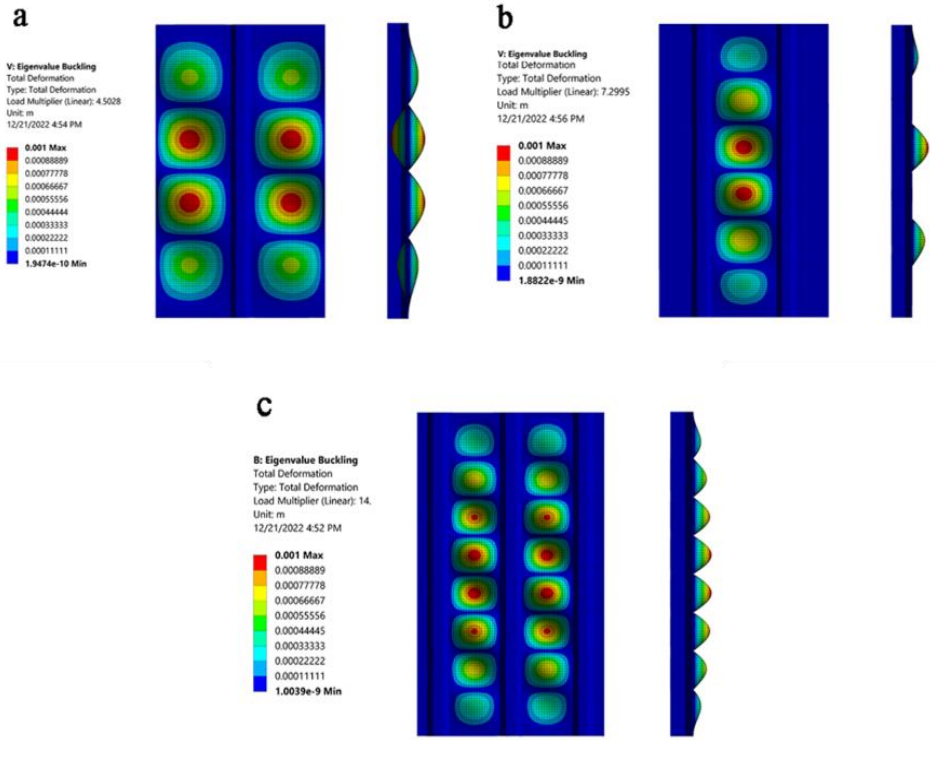

Fig. 22 First mode eigenvalue buckling contours: (a) Dist-1; (b) Dist-2; and (c) Dist-3.

© Engineered Science Publisher LLC 2024

compression and shear loads. The ultimate panel collapse load values and the total energy generated during the non-linear analysis are shown in Figs. 23(a) and (b), respectively. The graphs also illustrate the buckling collapse behaviour performance of stiffened panels with variations in the number and distance between stiffeners. In Fig. 23(a), the load–displacement graph indicates that the displacement change parallel to the y-axis of 25 mm corresponds to the change of buckling load received to reach a certain deformation value. In Fig. 23(b), the energy–displacement graph shows the total energy generated during buckling performance to achieve a displacement change of 25 mm.

In Fig. 23(a), it is shown that increasing the number of stiffeners and narrowing the distance between stiffeners increases the value of the ultimate panel collapse load significantly. Starting from the stiffened panel structure with one stiffener (Dist-1), which has the lowest buckling performance trend, adding stiffeners and spacing the stiffeners by 360 mm (Dist-2) increases the buckling performance considerably. With the addition of 3 stiffeners with a spacing distance of 280 mm (Dist-3), the buckling performance of the stiffened panels was significantly improved, until the ultimate buckling collapse load is sufficiently high. On the other hand, in Fig. 23(b), the total energy generated in the buckling performance of stiffened panels with variations in the number and spacing between stiffeners is shown. The energy–displacement graph shows the same reaction as the load–displacement graph. The difference in the number and distance between stiffeners greatly affects the total energy produced. In the same order, the lowest value was observed for Dist-1, then Dist-2, while the highest is observed for the Dist-3 variation. The Ultimate Panel Collapse and Total energy values are provided in Table 15.

Based on the data in Table 15, it was found that the value of the ultimate panel collapse load with stiffener variation Dist-3 had the highest value of 2973.2 kN, more than twice as high as the value with stiffener variation Dist-1 (1117 kN). The value of stiffener variation Dist-2 is 2038.5 kN, which was also higher than that of Dist-1, but lower than Dist-3. This means that the ultimate panel collapse load value increases with the distance between the stiffeners, as the Dist-2 variation had a distance of 200 mm. In comparison, the Dist-3 variation had a distance of 300 mm. The increase in the ultimate panel collapse load value starts with the Dist-2 variation, which increases by 82.4 % when compared to the Dist-1 variation, then the Dist-3 variation, which presents an additional increase of 45.85 % when compared to the Dist-2 variation. For the total energy produced, based on the data in Table 14, it was found that the value of total energy in the Dist-3 variation had the highest value of 61.61 kJ, which was also more than twice as high as the value for the Dist-1 variation (23.78 kJ). The value for the Dist-2 stiffener variation is 42.81 kJ, again placing it in between the Dist-1 and Dist-3 variations. This means that the total energy produced also increases with the distance between the stiffeners, as the Dist-2 variation has a distance of 200 mm, while the Dist-3 variation has a distance of 300 mm. The increase in the total value of energy produced starts with the Dist-2 variation, which increases by 80 % when compared to the Dist-1 variation, then the Dist-3 variation, which experiences an additional increase of 43.91 % when compared to the Dist-2 variation.

Table 15. Ultimate panel collapse load and total energy values.

Specimen	Ultimate Panel Collapse Load (kN)	Energy (kJ)
Dist-1	1117	23.78
Dist-2	2038.5	42.81
Dist-3	2973.2	61.61

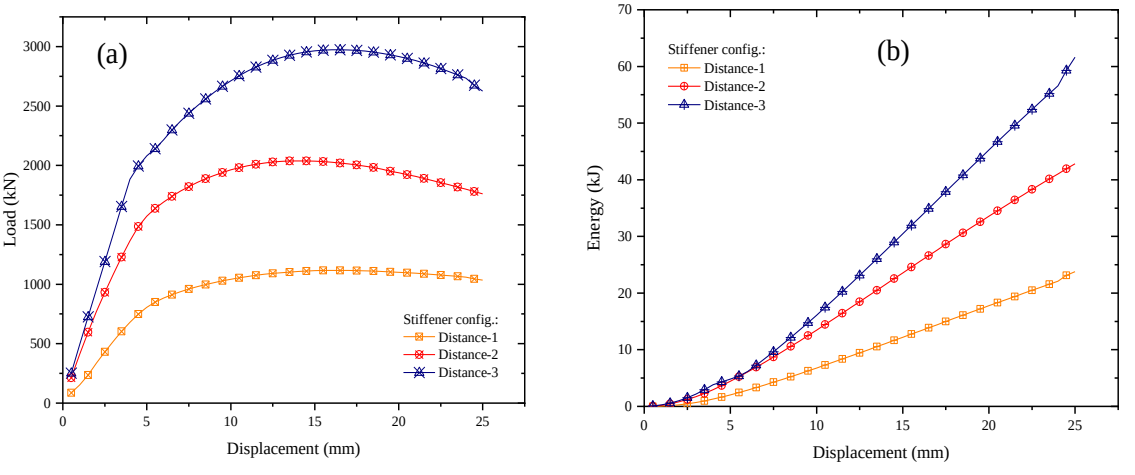

Fig. 23 Graphs of variation in the number and spacing of stiffeners: (a) load–displacement; and (b) energy–displacement.

© Engineered Science Publisher LLC 2024

The ultimate panel collapse load and total energy values generated from the three variations of stiffener spacings, shown in Figs. 23(a) and (b) and detailed in with Table 14, show a considerable difference in each variation, where each added stiffener increases the ultimate panel collapse load and total energy values by more than 40%. This indicates that, on the same plate, the addition and reduction of stiffeners greatly affect the buckling performance of stiffened panels, where the panel with the Dist-3 variation in this analysis presented the best buckling collapse behaviour performance when compared to the other variations. In the non-linear analysis, the equivalent contours of each stiffened panel with different stiffener spacings were also obtained. The contours displayed in this analysis are equivalent to the deformation and stress during buckling performance. The variation in stiffener spacing also affected the distribution of deformation and stress in the stiffened panels. Each stiffened panel was analysed at the three time steps of 0.35 s, 7 s, and 1 s. The equivalent deformation and stress contours are shown in Figs. 24 and 25, respectively.

In Fig. 24, the equivalent deformation contours of the stiffened panels with various spacings are shown. In Fig. 24(a), for stiffener variation Dist-1, it can be seen that deformation occurs at the beginning of the buckling performance, precisely centred at two points at 0.35 s. Then, at 0.7 s, it can be seen that the distribution of deformation in the stiffener and plate is quite large and still centred at these two points of deformation. Until the end of the buckling performance, the contours show deformation centred at the two points and the centre of the stiffened panels—more precisely, on the stiffener and the side of the plate parallel to the centre point—with the maximum deformation reaching 114.72 mm, this being the largest deformation produced compared to the other two variations. Then, for the variation Dist-2, shown in Fig. 24(b), the buckling performance differed from that of the previous variation due to the increase in the number of stiffeners on the plate. At the beginning, it is not clear that the deformation change is centred on the stiffened panel; however, at 0.7 s, it is clear that the deformation change and its distribution are centred on the middle of the stiffened panel. Then, at the end of the buckling performance test, the contour shows deformation centred on the middle stiffener, experiencing

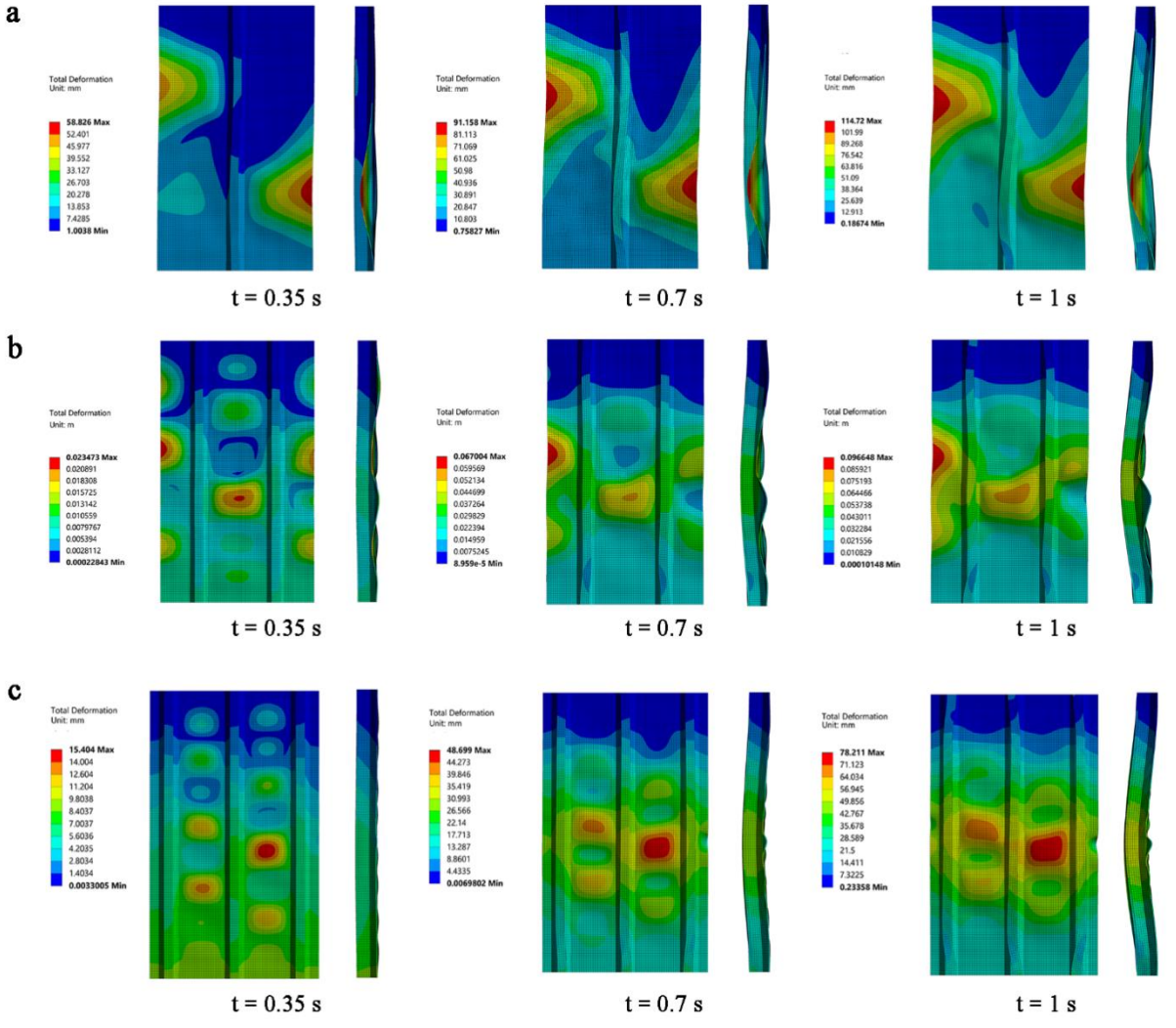

Fig. 24 Equivalent deformation contours of the specimens: (a) Dist-1; (b) Dist-2; and (c) Dist-3.

© Engineered Science Publisher LLC 2024

global buckling, and the side of the plate parallel to the centre point of the plate, with the maximum deformation in this variation reaching 96.64 mm.

For the last variation (Dist-3), where the number of stiffeners is increased and the distance between stiffeners is closer, which is shown in Fig. 24(c), at the beginning of the buckling performance test, there is still no visible change in deformation. However, at 0.7 s, there is an even and centralised distribution of deformation due to global buckling. Then, at the end, the stiffened panel deforms in a manner centred on the middle of the stiffened panel, with a maximum deformation reaching 78.21 mm, which is the smallest compared to the other two variations. This proves the previous statement: through adding and reducing the distance between stiffeners on the stiffened panel, the Dist-3 stiffener variation leads to the best buckling collapse behaviour performance, with minimal deformation produced.

In Fig. 25(a), the stress contours of the stiffener variation Dist-1 are shown. At 0.35 s, the stress distribution is still centred on the stiffener and is not clearly visible on the plate. Then, at 0.7 s, the stress distribution occurred on the plate, centred on the middle side of the stiffened panel. Until the end of the buckling performance test, the stress distributed at the centre of the stiffened panel increased along with the deformation formed, with the maximum stress reaching

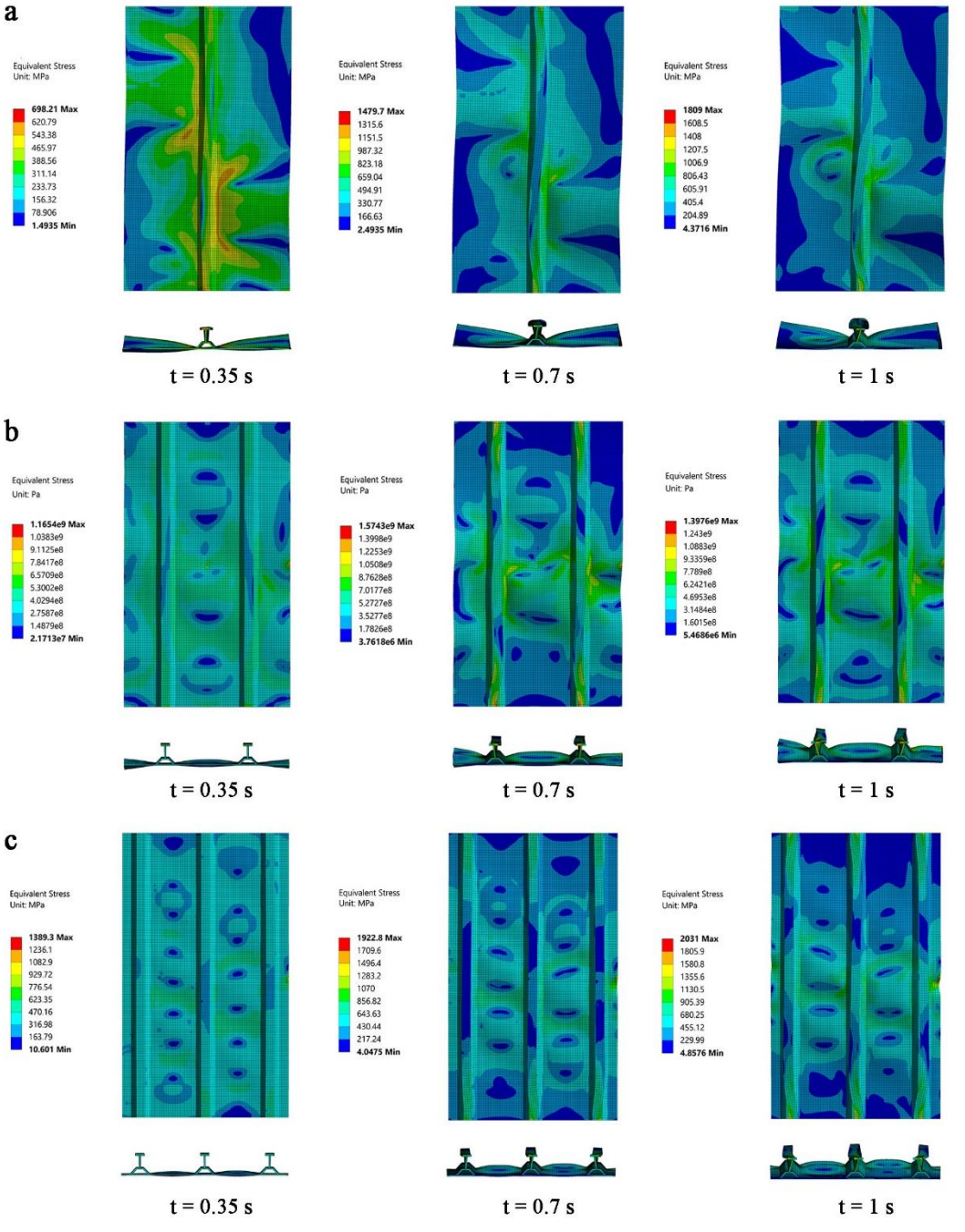

Fig. 25 Equivalent stress contours of specimens: (a) Dist-1; (b) Dist-2; and (c) Dist-3.

© Engineered Science Publisher LLC 2024

1809 MPa.

In Fig. 25(b), the stress contours for the variation Dist-2 are shown, where the stiffeners are provided on the panel to prevent buckling collapse. In the initial stage of the buckling performance test, no visible stress distribution was concentrated on the stiffened panel structure; this is due to the increase in the number of stiffeners, which enhances the buckling resistance. However, at 0.7 s, the stress distribution started to appear in the middle of the stiffened panel and the deformation formed, indicating the onset of local shell buckling. At the end of the buckling performance, the stress distribution was also centred in the middle of the stiffened panels, with maximum stress reaching 1397.6 MPa, accompanied by a large deflection and sideways distortion of the stiffeners. In contrast, as shown in Fig. 25(c), for the last variation, Dist-3, at the beginning of the buckling performance test, the stress distribution on the stiffener was still not visible or centred on certain parts, due to the sliding stiffeners not being welded to the shell. At 0.7 s, the stress distribution can be seen to be evenly distributed throughout the section due to the occurrence of global buckling in the stiffened panel with the Y-type stiffener variation. Then, at the end of the buckling performance test, the stress was evenly distributed throughout the section, with the maximum stress centred on the middle of the stiffened panel structure. Due to global buckling, the maximum stress of the entire stiffened panel structure, centred in the middle, reached 2031 MPa.

8. Comparison of results with stiffener configuration variations

The stiffener configurations used on the stiffened panel structure included six different stiffener configuration modes: one transversal and one longitudinal cross-stiffener, one transversal and two longitudinal cross-stiffeners, two transversal and two longitudinal cross-stiffeners, three transversal and one longitudinal cross-stiffener, and three transversal and two longitudinal cross-stiffeners. The stiffened panels were analysed using Y-type stiffeners, which was the stiffener type that presented the best buckling collapse behaviour performance in the previous analysis. The buckling collapse behaviour analysis was assessed starting from the critical buckling load value in the linear analysis, then through non-linear analysis according to the ultimate panel collapse load value from the load–displacement graph and the total energy generated in the energy–displacement graph.

8.1 Linear analysis

In the linear analysis of the stiffened panel structure with variations in stiffener configuration, the values of the critical buckling load with respect to the variations in the cross-stiffener configuration, where the stiffeners are configured crosswise, are shown in Table 16. First, the stiffened panel with one transverse stiffener and one longitudinal stiffener (Config-1) had a critical buckling load value of 515,940 N/m. Then, when adding two longitudinal stiffeners (Config-2), the critical buckling load increases to 596,890 N/m; meanwhile, with one longitudinal stiffener but two transverse stiffeners (Config-3), a critical buckling load value of 823,020 N/m was obtained. Adding another longitudinal stiffener, for two transverse stiffeners and two longitudinal stiffeners (Config-4), the critical buckling load value increased to 941,140 N/m. Then, for the configuration with three transverse stiffeners and one longitudinal stiffener, a critical buckling load value of 1,494,200 N/m was obtained. In the last variation, another longitudinal stiffener was added, for three transverse stiffeners and two longitudinal stiffeners, where the critical buckling load value increased to 1,562,400 N/m.

Table 16. Effect of stiffener configuration variation on critical buckling load.

Specimen	Critical Load (N/m)
Config-1	515,940
Config-2	596,890
Config-3	823,020
Config-4	941,140
Config-5	1,494,200
Config-6	1,562,400

With the data in Table 16, it can be interpreted that, in the cross-stiffener configuration (similar to the analysis in the previous sub-chapter), the addition of stiffeners affects the critical buckling load value under axial load. The addition of a longitudinal stiffener increased the critical buckling load value by 15.68 % in the comparison between the Config-2 and Config-1 variations. Likewise, the Config-4 variation increased the value by 14.35 %, compared to the Config-3 variation; while the Config-6 variation increased the critical buckling load value by 4.56 % compared to Config-5. At the same time, the addition of a transverse stiffener increased the critical buckling load value by 82.41 % in the comparison between Config-3 and Config-1 variation. Likewise, the Config-5 variation increased the critical buckling load value by 58.76 % compared to Config-3. A more detailed comparison is shown in Fig. 26.

The results presented in Table 16 and Fig. 26 show the effect of adding stiffeners in different configurations on the critical buckling load of the panels under axial load. One of the main findings is that the cross-stiffener configuration, which involves adding a transverse stiffener perpendicular to

 © Engineered Science Publisher LLC 2024

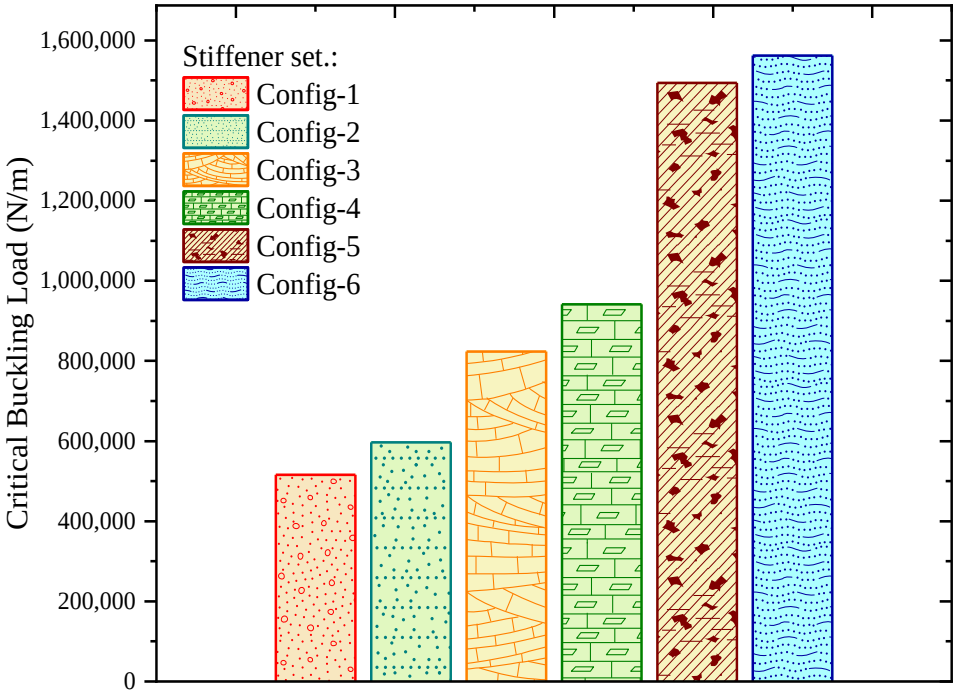

Fig. 26 Comparison of critical buckling load values under stiffener configuration variations.

the longitudinal stiffeners, led to a significant increase in the critical buckling load value, with an increment of more than 50% observed in the stiffener configuration analysis. This can be attributed to the enhanced resistance of the panel to out-of-plane deformation due to the presence of transverse stiffeners. On the other hand, the addition of a longitudinal stiffener parallel to the existing ones did not result in a substantial increase in the critical buckling load value, with only a 5% increment or less detected with this variation of stiffener configuration. This is because longitudinal stiffeners mainly affect the in-plane stiffness of the panel, which is not the governing factor for buckling under axial load.

The contours of the first eigenvalue mode buckling of stiffened panels with varying configurations of stiffeners are depicted in Fig. 27. In this figure, the contours of the eigenvalue buckling modes for each cross-stiffener configuration variation are shown. The addition of a transverse stiffener to the cross-stiffener configuration, as in Figs. 27(a), (b), and (c), affects the eigenvalue contour in terms of where the increasing waveform formed on the structure, thus increasing the critical buckling load and buckling resistance performance. The addition of a longitudinal stiffener to the cross-stiffener configuration, as in Figs. 27(a) and (b), it looks a little different as the waveform is not formed in the middle of the structure or, more precisely, between two longitudinal stiffeners, such that the buckling performance in the middle of the structure is relatively low. Although it strengthens the buckling resistance of the structure, due to the uneven distribution of the buckling load, the increase in the value of the critical buckling load is not too large or effective. Likewise, the addition of longitudinal stiffeners are reflected in the variations shown in Figs. 27(c)–(f).

8.2 Non-linear analysis

In the non-linear analysis of the stiffened panel structure with variations in stiffener configuration, the ultimate panel collapse load results are shown in Fig. 28(a) and the total energy generated is shown in Fig. 28(b).

The buckling collapse behaviour performance of stiffened panels with various stiffener configurations is shown in Figs. 28 (a) and (b). The load–displacement graph shows the change of displacement (deformation) parallel to the y-axis of 25 mm, which shows the change of buckling load received to reach a certain deformation value. The energy–displacement graph shows the total energy generated during buckling performance to achieve a displacement change of 25 mm.

In Fig. 28(a), it is shown that the addition of a transverse stiffener to the plate has a major effect on buckling performance, as can be observed for the Config-1, Config-3, and Config-5 variations. Due to the axial load applied to the stiffened panel structure, the addition of transverse stiffeners will have a major effect on buckling resistance and simultaneously increase the ultimate panel collapse load. At the same time, the addition of a longitudinal stiffener does not have much effect on the axial load applied to the stiffener structure. However, in the comparison between Config-1 and

© Engineered Science Publisher LLC 2024

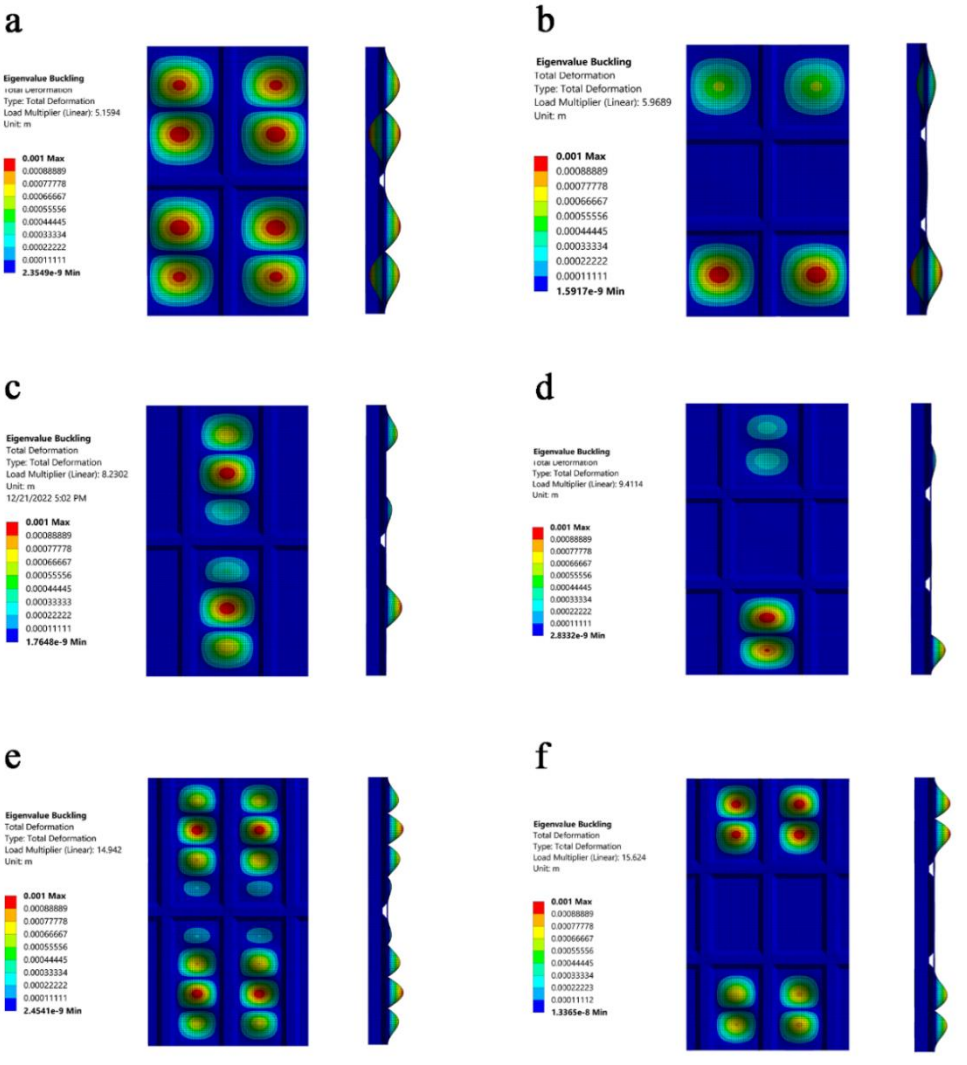

Fig. 27 First mode eigenvalue buckling shapes: (a) Config-1; (b) Config-2; (c) Config-3; (d) Config-4; (e) Config-5; and (f) Config-6.

Config-2 variations, the addition of longitudinal stiffeners increased the stiffness of the plate structure due to the unequal ratio of the number of stiffeners, thus reducing the value of the ultimate collapse load. Similar phenomena occurred for the Config-5 and Config-6 variations. On the other hand, in the Config-3 and Config-4 variations, the addition of longitudinal stiffeners makes the stiffener ratio the same as two transverse stiffeners and two longitudinal stiffeners, such that the value

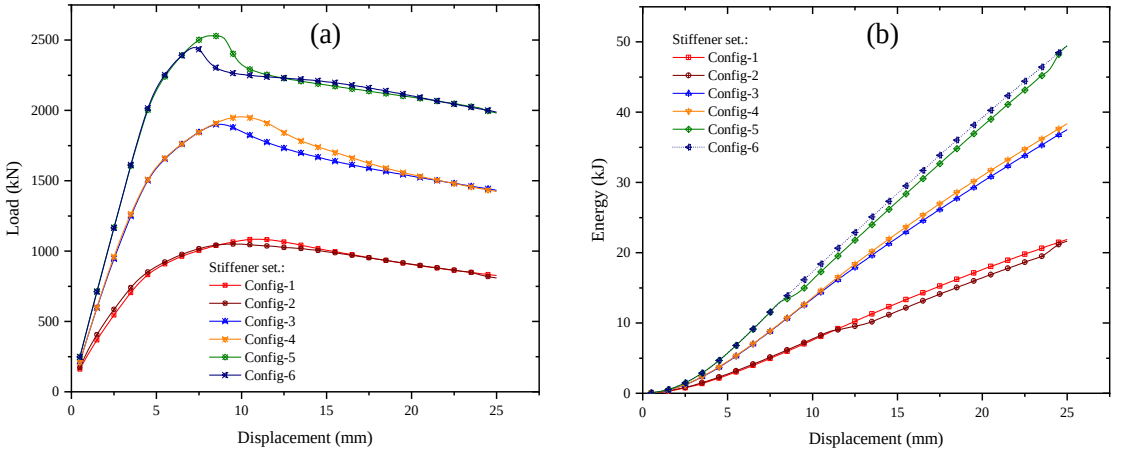

Fig. 28 Graphs of variation in stiffener configuration: (a) load–displacement; and (b) energy–displacement.

© Engineered Science Publisher LLC 2024

of the ultimate panel collapse load increased.

In Fig. 28(b), the total energy generated in the buckling performance of stiffened panels with various stiffener configurations is shown. The energy–displacement graph shows the same reaction as the load–displacement graph, where the addition of transverse stiffeners increased the total energy value produced, as can be seen in the comparison between Config-1, Config-3, and Config-5. However, the addition of longitudinal stiffeners also reduced the total energy value produced, due to a lower collapse point, which can be seen in the comparison of variations Config-1 and Config-2, along with variations Config-5 and Config-6. In the comparison between Config-3 and Config-4, an increase in total energy occurred due to an increase in the collapse point. The Ultimate Panel Collapse and Total Energy values are summarised in Table 17.

Table 17. Ultimate panel collapse load and total energy values.

Specimen	Ultimate Panel Collapse Load (kN)	Energy (kJ)
Config-1	1085.1	21.9
Config-2	1050	21.67
Config-3	1899.8	37.5
Config-4	1955.3	38.35
Config-5	2529.6	49.47
Config-6	2439.7	49.46

The data in Table 17 demonstrate how the presence and orientations of stiffeners affect the ultimate panel collapse load of the different configurations. In particular, the addition of longitudinal stiffeners reduced the value of the ultimate panel collapse load in the comparison between Config-1 and Config-2. Config-1, which has an ultimate panel collapse value of 1085.1 kN, was superior to the Config-2 variation (1050 kN, or decreased by about 3.2 %). A similar case also occurred in the comparison between Config-5 and Config-6, where the ultimate panel collapse load value of Config-5 (2529.6 kN) decreased due to the addition of longitudinal stiffeners in the Config-6 variation (to 2439.7 kN, about 3.55 % lower). However, the addition of longitudinal stiffener variations between Config-3 and Config-4 showed a different reaction, where the ultimate panel collapse value in the Config-3 variation was 1899.8 kN, which increased after the addition of a longitudinal stiffener in the Config-4 variation to 1955.3 kN (for an increase of about 2.92 %). The addition of transverse stiffeners showed a different response, where each added transverse stiffener increased the ultimate panel collapse load value. In the Config-3 variation, the ultimate panel collapse load increased by about 75.08% compared to the Config-1 variation; meanwhile, in the Config-5 variation, the ultimate panel collapse load increased by about 33.15 % compared to Config-3.

For the total energy generated, based on the data in Table 17, it can be seen that the addition of a transverse stiffener also affected the total energy generated. Similar to the ultimate panel collapse value, the total energy value increased when a transverse stiffener was added. However, Config-1 variation had a total energy generated of 21.9 kJ, which decreased when a longitudinal stiffener was added (as in the Config-2 variation) to 21.67 kJ (or about 1.05% lower). The same case occurred when adding a longitudinal stiffener from Config-5 to Config-6, where the Config-5 variation had a total energy of 49.7 kJ, which decreased to 49.46 kJ (about 0.48% lower) under the Config-6 variation. However, for the Config-3 and Config-4 variations, the addition of a longitudinal stiffener increased the total energy value: in Config-3, the total energy was 37.5 kJ, increasing in the Config-4 variation to 38.35 kJ (about 2.28 % higher). The addition of transverse stiffeners presented a different reaction, where each added transverse stiffener increased the total energy value. In the Config-3 variation, the total energy increased by about 71.23 % compared to the Config-1 variation; meanwhile, in the Config-5 variation, the total energy increased by about 32.53 % compared to Config-3. In the non-linear analysis, the equivalent contours of each stiffened panel with various stiffener configurations were also obtained. The contours displayed in this analysis are the contours equivalent to the deformation and stress during buckling performance testing. The variation of each stiffener configuration also affected the distribution of deformation and stress in the stiffened panels. Each stiffened panel was analysed at the three time steps of 0.35 s, 7 s, and 1 s. The equivalent deformation contours and deformation distribution under each stiffener configuration variation are shown in Figs. 29 and 30, respectively.

In Fig. 29(a), showing the Config-1 variation, at the beginning of the buckling performance, slight deformation was observed. Then, at 0.7 s, the deformation began to be centred in the middle, or on the longitudinal stiffener. Then, at the end of the buckling performance test, the deformation was centred in the middle of the structure with a total maximum deformation of 80.12 mm. In Fig. 29(b) for variation Config-2, the addition of a longitudinal stiffener caused the deformation distribution to differ from that of the previous variation. At the beginning of the buckling performance test, a little deformation was observed; precisely on one of the longitudinal stiffeners. Then, at 0.7 s, the deformation began to be centred around the longitudinal stiffener at the bottom of the structure. At the end of the buckling performance test, the deformation was centred at the bottom of the structure, with a

© Engineered Science Publisher LLC 2024

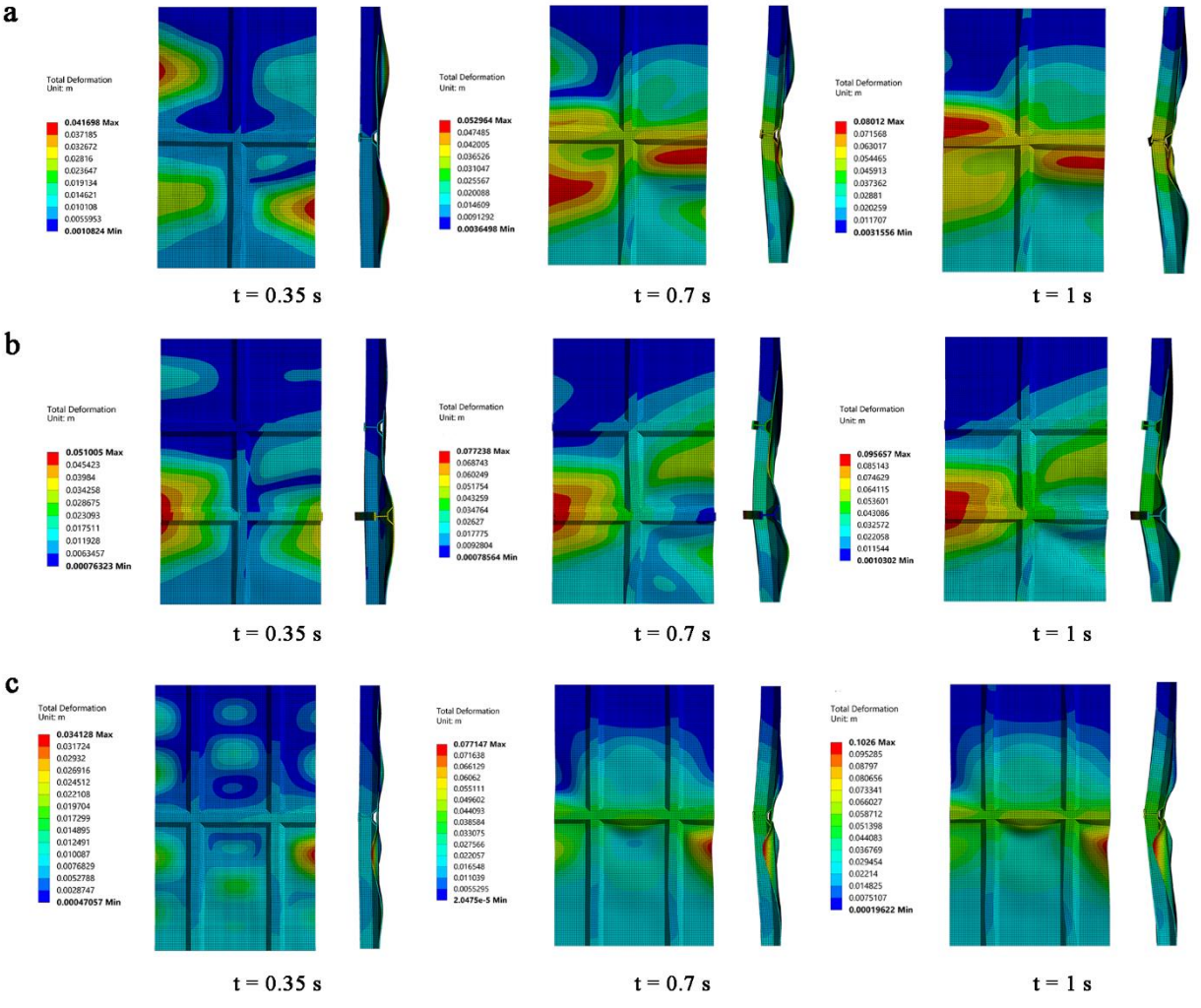

Fig. 29 Equivalent deformation contour of specimens: (a) Config-1; (b) Config-2; and (c) Config-3.

total maximum deformation of 95.65 mm. The variation Config-3, as shown in Fig. 29(c), has a transverse stiffener that affects the deformation distribution. The buckling performance did not show any visible deformation at first. Then, at 0.7 s, a small deformation appeared around the longitudinal stiffener in the centre. Finally, the deformation spread to the centre and sides of the structure, with a maximum value of 102.6 mm.

The variation Config-4, shown in Fig. 30(a), has a longitudinal stiffener that makes the structure more proportional and effective in distributing deformation. The buckling performance did not show any deformation at first. Then, at 0.7 s, the deformation moved to the longitudinal stiffener at the bottom of the structure. Finally, the deformation was focused on the bottom of the structure, with a maximum value of 68.7 mm. The transverse stiffener added to variation Config-5, shown in Fig. 30(b), changes how the deformation spreads and increases the plate structure's rigidity. The deformed part was not seen at the start of the buckling performance test. However, a small deformation started to appear around the longitudinal stiffener or in the centre after 0.7 s. The deformation reached its peak at the end of the buckling performance test, with a total maximum deformation of 74.01 mm on the sides and centre of the structure.

As shown in Fig. 30(c), for variation Config-6, the addition of a longitudinal stiffener causes the plate structure to have the highest stiffness, compared to other variations. At the beginning of the buckling performance, the deformation of the structure was not observed. Then, at 0.7 s, the deformation began to become centred on the longitudinal stiffener at the bottom of the structure. Then, at the end of the buckling performance test, the deformation was centred at the bottom of the structure, with a total maximum deformation of 69.82 mm (the smallest among all of the variations). The equivalent stress contours for the stiffener configuration variations and stress distribution of each stiffener configuration variation are shown in Figs. 31 and 32. Notably, variations with one longitudinal stiffener-namely, Config-1, Config-3, and Config-5-had almost similar stress distributions. Starting from the beginning of the buckling performance test, the stress

 © Engineered Science Publisher LLC 2024

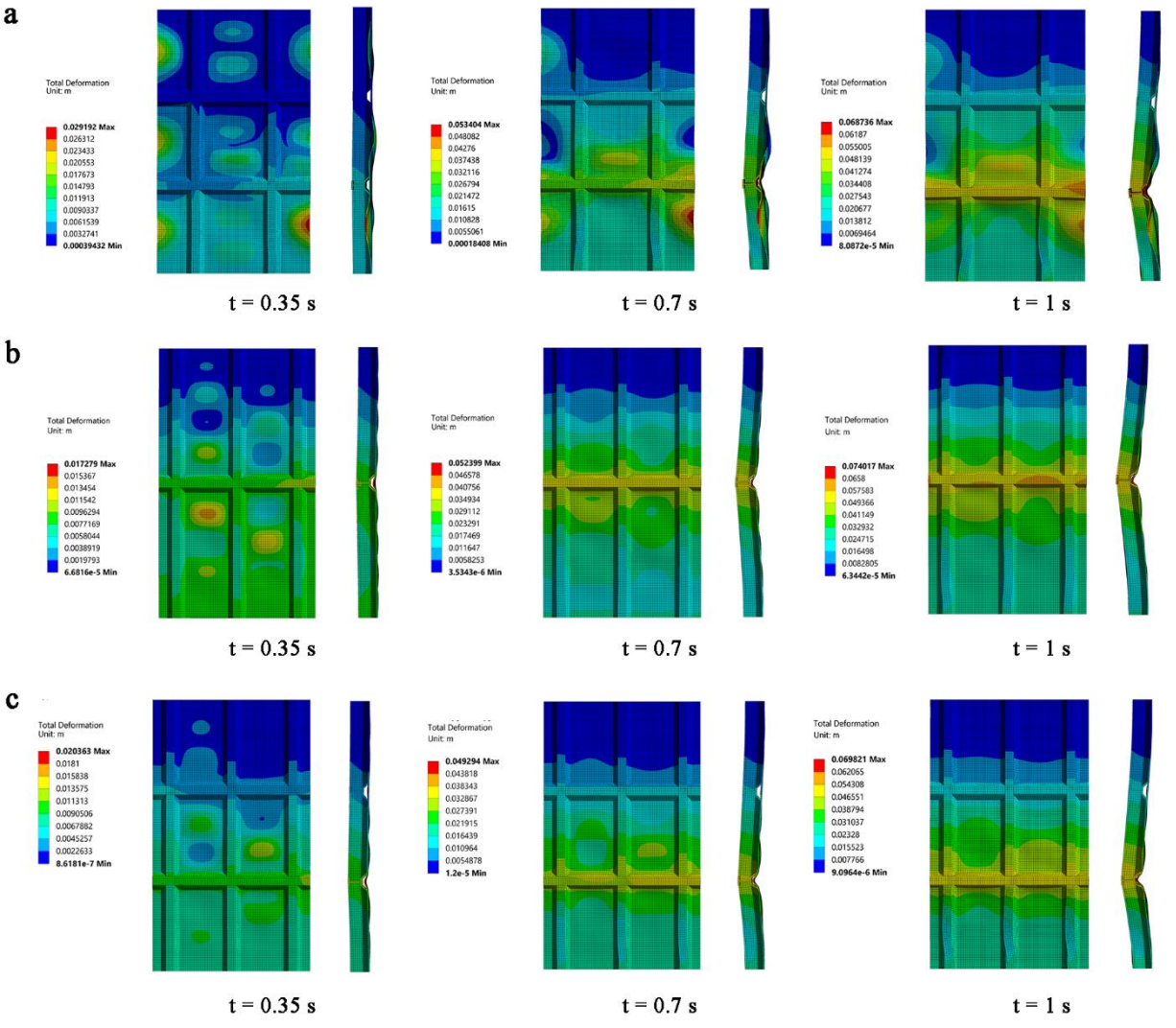

Fig. 30 Equivalent deformation contours of the specimens: (a) Config-4; (b) Config-5; and (c) Config-6.

distribution was still evenly distributed throughout the structure. Then, at 0.7 s, the stress distribution began to be centred in the middle of the structure; namely, on the longitudinal stiffener. Until the end of the buckling performance, the stress remained centred in the structure.

In variations with two longitudinal stiffeners-namely, Config-2, Config-4, and Config-6-there was also an almost similar stress distribution in each variation. Starting from the beginning of the buckling performance test, the stress distribution was evenly distributed throughout the stiffened panel structure. Then, at 0.7 s, the stress distribution began to be centred at the bottom of the structure; precisely, at the bottom longitudinal stiffener. At the end of the buckling performance test, the stress was centred at the bottom of the structure.

9. Yield results and mesh variation

The mesh size used in the stiffened panel structure model ranged from 10 mm to 100 mm. For the stiffened panels, Y-type stiffeners were used, which is the stiffener type with the best buckling collapse behaviour in the previous analysis. The buckling behaviour was assessed starting from the critical buckling load value in the linear analysis, then in the non-linear analysis according to the ultimate panel collapse load value from the load–displacement graph, and the total energy generated in the energy–displacement graph.

9.1 Linear analysis

The effect of varying mesh size on the buckling performance in the linear analysis of stiffened panel structures is presented in Table 18. As the mesh size increases, the simulation results become less accurate and the critical buckling load value increases. Table 18 also displays the critical buckling load value and the percentage difference in value with respect to a mesh size of 10 mm (or a mesh size that has an error below 1 %, see the reference validation analysis for more details).

© Engineered Science Publisher LLC 2024

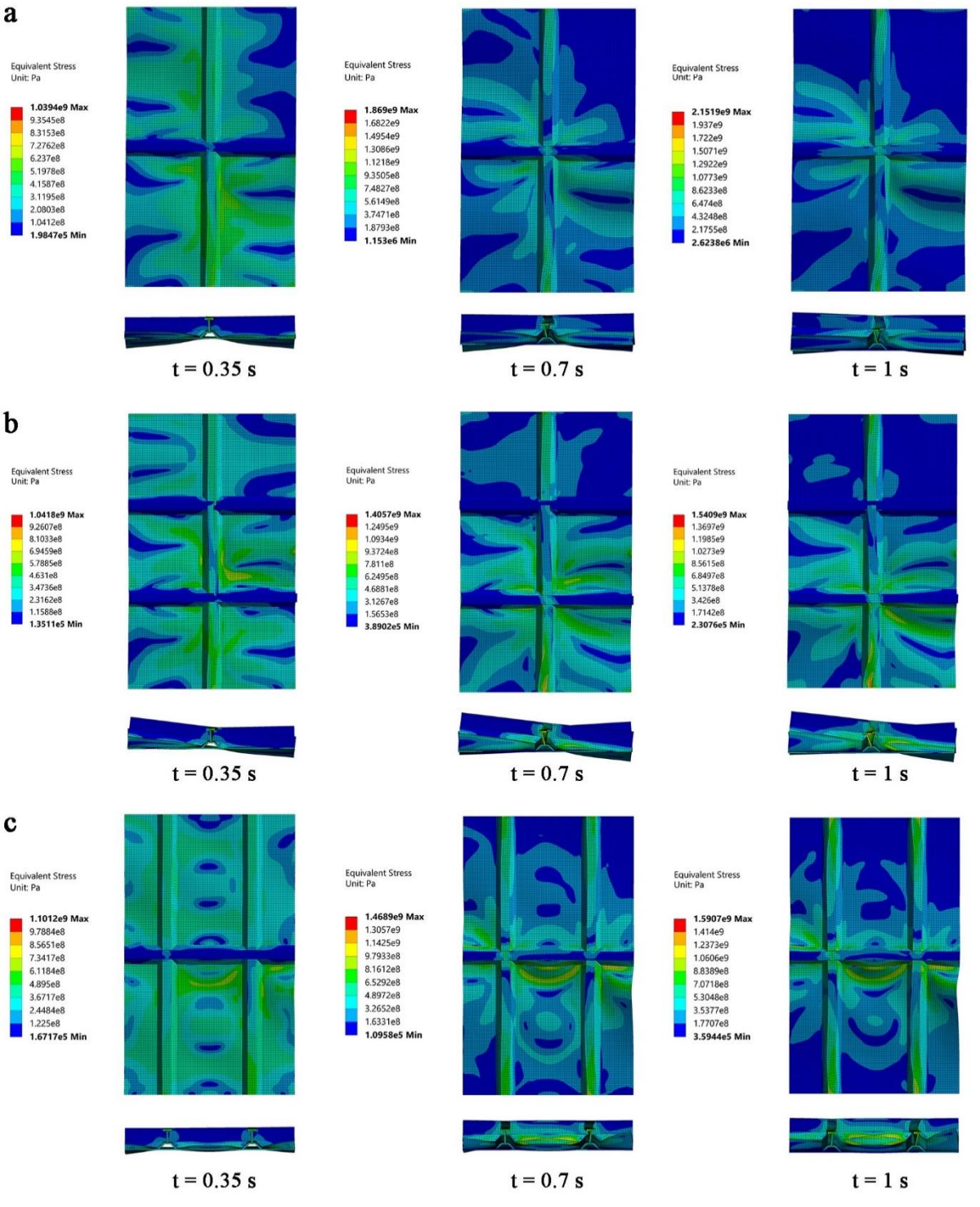

Fig. 31 Equivalent stress contours on the specimens: (a) Config-1; (b) Config-2; and (c) Config-3.

The derived formulation based on the depicted data in Table 18 was obtained as $y = (1.02064 \times 10^6) + 14222.90909x$.

The mesh sizes that had an error below 10% were the same as used in the previous experimental validation (*i.e.*, below 60 mm). The simulation results for the stiffened panel with a 10 mm mesh size were used as a reference. The simulation results increased gradually with the mesh size until they reach a difference of 101.36 % from the reference. The critical buckling load was obtained by applying the eigenvalue buckling solution method to the linear analysis, which provides the eigenvalue buckling modes and their corresponding contours. Fig. 33 shows how the eigenvalue buckling contours varied for the two different mesh sizes of 10 mm and 70 mm, as the reference validation analysis indicated that a mesh size larger than 50 mm leads to an error greater than 10 %.

 © Engineered Science Publisher LLC 2024

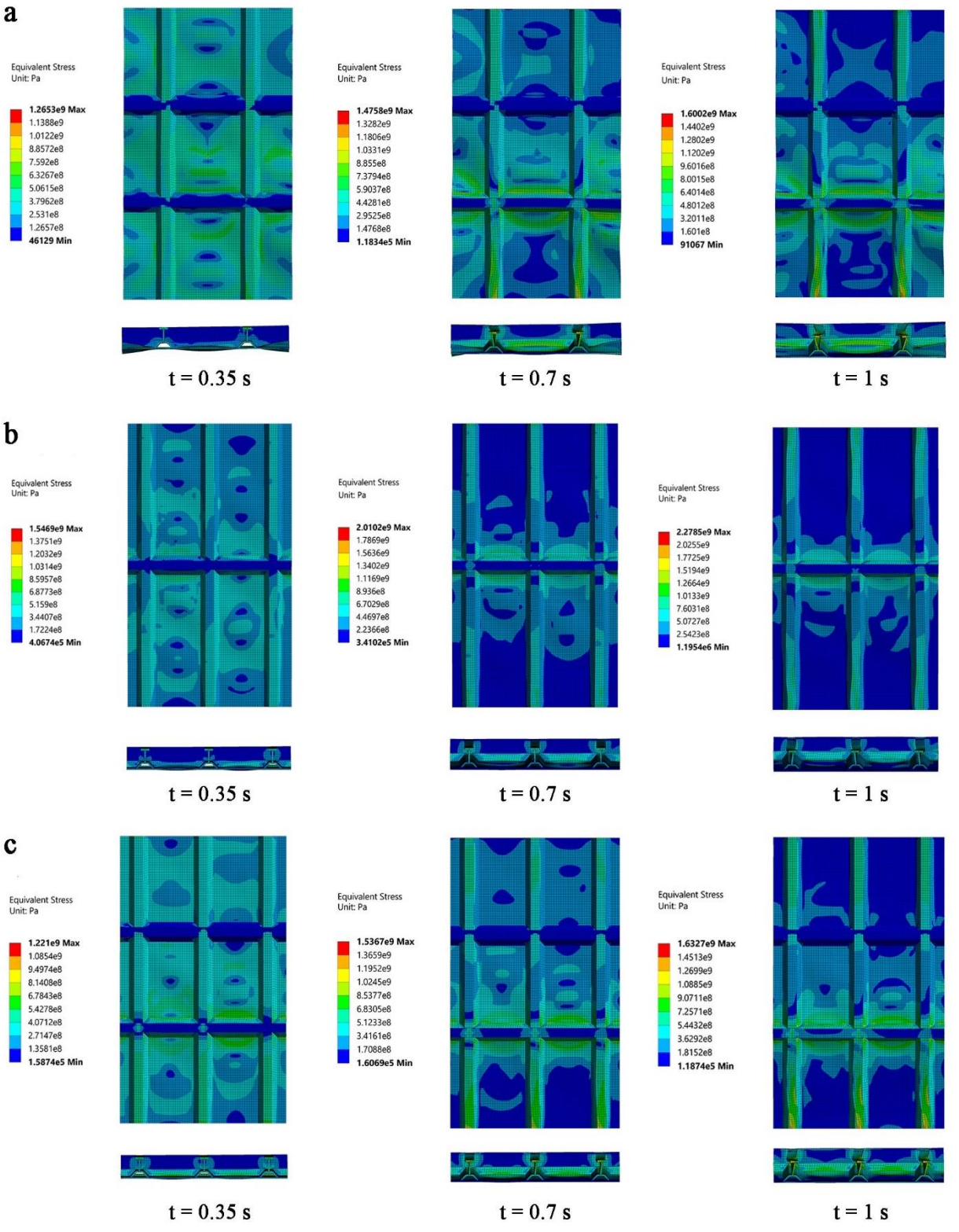

Fig. 32 Equivalent stress contours on the specimens: (a) Config-4; (b) Config-5; and (c) Config-6.

The effect of mesh size on the buckling eigenvalue contours is shown in Fig. 33. The buckling eigenvalue contour is a graphical representation of the theoretical buckling strength of an ideal linear elastic structure. The smaller mesh size (10 mm) produced a more stable and accurate buckling eigenvalue contour, as seen in Fig. 33 (a). On the other hand, the larger mesh size (70 mm) resulted in an imperfect and inaccurate buckling eigenvalue contour, reducing the buckling

© Engineered Science Publisher LLC 2024

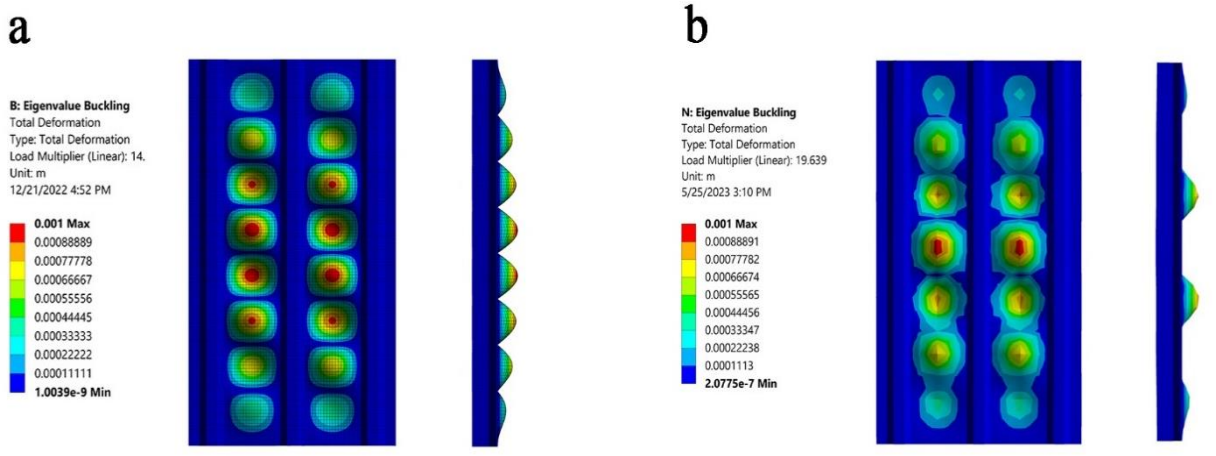

Fig. 33 First mode shape eigenvalue buckling: (a) 10 mm mesh; and (b) 70 mm mesh.

Table 18. Effect of mesh size on critical buckling load.

Specimen	Critical Load (N/m)	Percentage difference (%)
Mesh-10	1,400,000	-
Mesh-20	1,400,400	0.03
Mesh-30	1,416,900	1.21
Mesh-40	1,413,100	0.94
Mesh-50	1,528,300	9.16
Mesh-60	1,593,200	13.80
Mesh-70	1,963,900	40.28
Mesh-80	2,235,700	59.69
Mesh-90	2,819,100	101.36
Mesh-100	2,258,400	61.31

performance and causing a significant difference in the critical buckling load. Therefore, the mesh size should not exceed 50 mm for this analysis.

9.2 Non-linear analysis

The non-linear analysis of the stiffened panel structures with various mesh sizes yielded the result shown in Figs. 34(a) and (b); in particular, Fig. 34(a) displays the ultimate panel collapse load value, while Fig. 34(b) shows the total energy generated. The load-displacement and energy-displacement graphs for the different mesh sizes of the stiffened panel model are also presented in these figures. The buckling performance was similar across the mesh sizes, and each value was close to the variation with a 10 mm mesh size. The differences between the ultimate panel collapse load and the total energy values are illustrated in Fig. 35.

As shown in Fig. 35, there was no significant difference in the ultimate panel collapse load and total energy values with a mesh size ranging from 10 mm to 40 mm. This is consistent with the validation analysis, which revealed that this mesh size range led to the highest performance with a very low error rate. Table 19 indicates that the variation in mesh size from 10 mm to 40 mm resulted in less than 1% difference in the ultimate panel collapse load and total energy values, suggesting that this mesh size range yields fairly precise data. However, the non-linear analysis revealed that the load and energy values did not considerably differ, and the average was still under 10%. The derived formulation based on the ultimate collapse load in Fig. 35 (a) is presented as y = 2901.73333 +

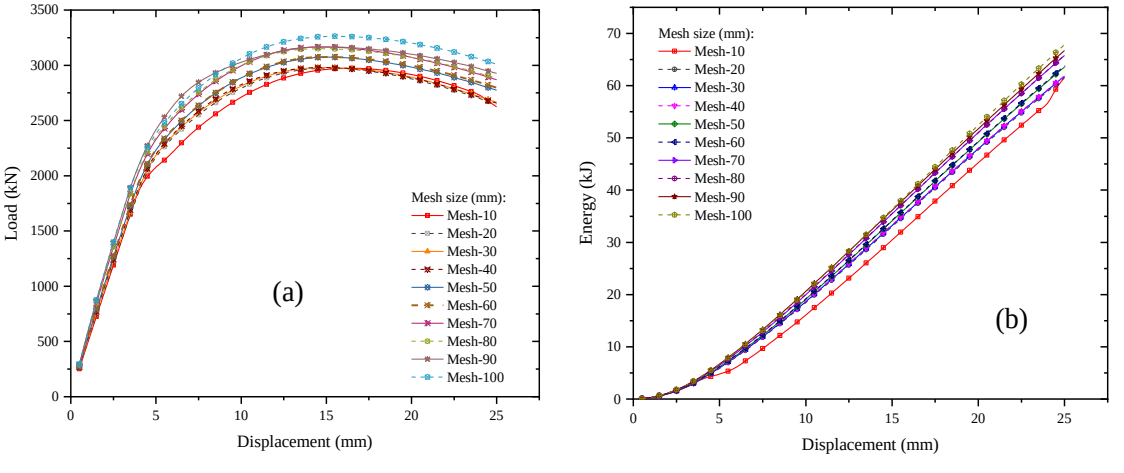

Fig. 34 Graphs of variation in mesh size: (a) load–displacement; and (b) energy–displacement.

© Engineered Science Publisher LLC 2024

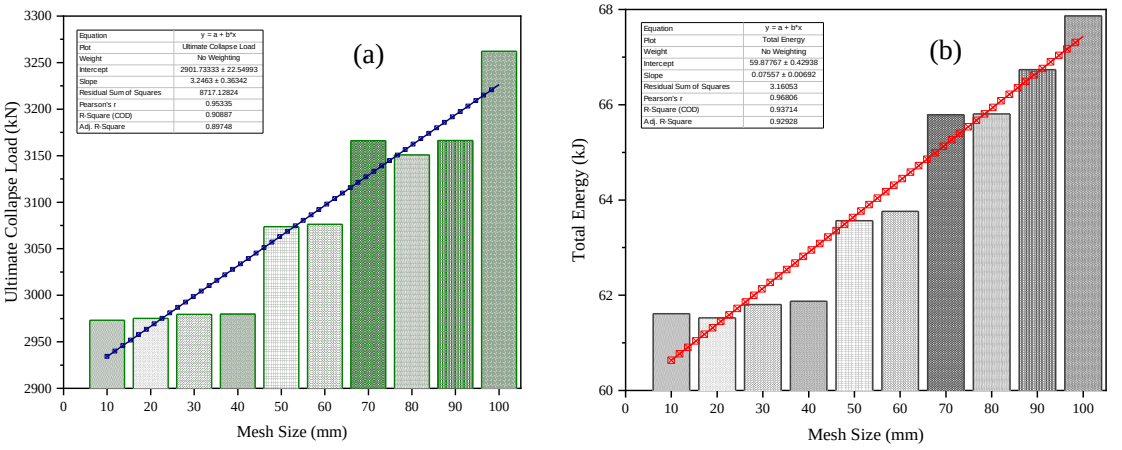

Fig. 35 Mesh convergence of (a) ultimate collapse load and (b) total energy.

Table 19. Ultimate panel collapse load and total energy values.

Specimen	Ultimate Panel Collapse Load (kN)	Energy (kJ)	Percentage Difference (%)	
			Load	Energy
Mesh-10	2973.2	61.613	-	-
Mesh-20	2975.2	61.524	0.07	-0.14
Mesh-30	2979.5	61.804	0.21	0.31
Mesh-40	2979.8	61.876	0.22	0.43
Mesh-50	3073.6	63.567	3.38	3.17
Mesh-60	3076.2	63.761	3.46	3.49
Mesh-70	3166.1	65.788	6.49	6.78
Mesh-80	3150.7	65.807	5.97	6.81
Mesh-90	3166.2	66.738	6.49	8.32
Mesh-100	3262.3	67.863	9.72	10.14

3.2463x, while the total energy in Fig. 35(b) gives y = 59.87767 + 0.07557x.

In the non-linear analysis, the equivalent contours for each stiffened panel with various mesh configurations were also obtained. The contours displayed in this analysis are equivalent to the deformation and stress during buckling performance contours, and the variation in mesh configuration also affects the distribution of deformation and stress in the stiffened panels. Each stiffened panel was analysed at three time steps; namely, 0.35 s, 7 s, and 1 s. The differences

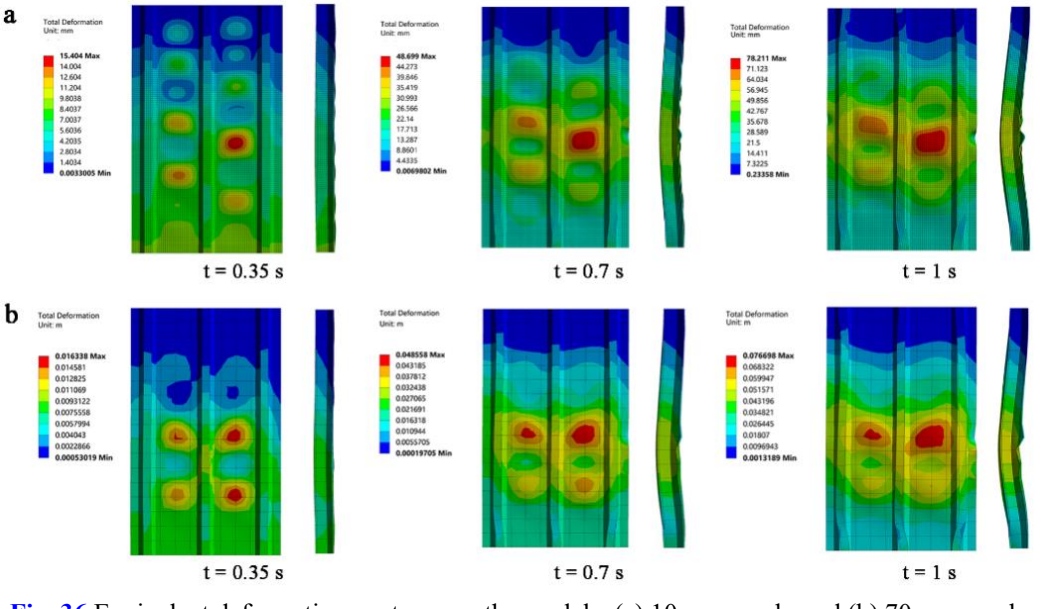

Fig. 36 Equivalent deformation contours on the models: (a) 10 mm mesh; and (b) 70 mm mesh.

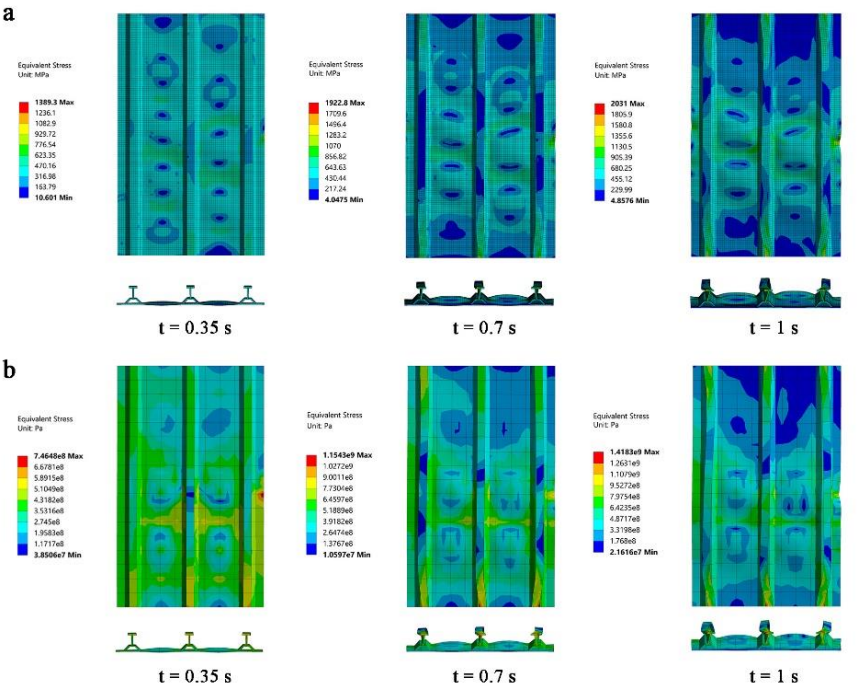

Fig. 37 Equivalent stress contours on the models: (a) 10 mm mesh; and (b) 70 mm mesh.

between the equivalent contours of deformation and stress under the 10 mm and 70 mm mesh size variations are shown in Figs. 36 and 37, respectively.

From Figs. 36 and 37, it can be seen that, even with different mesh sizes, all variations had similar deformation and stress distributions. The structure of stiffened panels with Y-type stiffeners provides stiffness that can cause global buckling, such that the distribution of deformation and stress will be centred in the middle of the stiffened panel structure, and the mesh size does not have a significant effect.

10. Conclusions

This study investigated buckling phenomena in stiffened panel structures for use in aircraft, considering various parameters including numerical parameters (mesh size) and physical parameters (stiffener type, stiffener spacing, and stiffener configuration). The Finite Element Method implemented in ANSYS Workbench was utilised for the analysis. The obtained research results led to the following conclusions:

1. Among the different stiffener types, the Y-type stiffener structure exhibited the highest resistance to buckling, displaying the best buckling behaviour. The T- and L- stiffener types follow the Y-type, while the I-type exhibited the lowest resistance. The Y-type stiffener displayed sufficient stiffness to induce global buckling. Additionally, the introduction of a transverse stiffener and a longitudinal stiffener at the stress centre effectively improve the buckling resistance under axial loading.
2. Concerning the variation in the number and spacing between stiffeners, the Dist-3 structure exhibited the highest buckling resistance, whereas the Dist-1 structure displayed the lowest buckling resistance.
3. The Config-5 structure demonstrated the highest buckling resistance. Conversely, the Config-2 structure exhibited the lowest buckling resistance, due to the reduction in the ultimate panel collapse load caused by the addition of longitudinal stiffeners.
4. In the reference validation and analysis of mesh size variations, a mesh size of 10 mm yielded the smallest error (< 1 %), when compared to the experimental data. Increasing the mesh size results in a higher error in the simulation data.

Investigating thin-walled structures in aircraft, particularly stiffened panels, is crucial due to the potential for catastrophic damage and losses resulting from buckling failures. Further research can be conducted using numerical simulations with various loading methods and boundary conditions. Additionally, the development of alternative lightweight materials should be explored, moving beyond traditional steel-based structures. Furthermore, studies should focus on specific structural components, such as fuselage, wings, or tails, that employ thin-walled structures. Finally, emphasis should be placed on the load distribution and the development of robust, lightweight structures with a wide range of configurations. Consideration of accidental loadings, such as impact with flying objects or creatures and collision during landing (referring to the critical flight stage), may be considered to

 © Engineered Science Publisher LLC 2024

facilitate a comprehensive point-of-view regarding the structural safety of the aircraft, especially in terms of civil airlines. Finally, with a wide range of configurations, focus can be placed on the load distribution for the development of strong, lightweight structures.

Acknowledgment
Not applicable.

Conflict of Interest
There is no conflict of interest.

Supporting Information
Not applicable.

Nomenclatures
a and *b* Length of the unloaded plate and the length of the loaded plate, respectively
CPT Classical Thin Plate Theory
D Flexural rigidity of the slab
E Young's Modulus
FEA Finite Element Analysis
h Thickness of the plate
ICAO International Civil Aviation Organization
k_c Buckling coefficient whose value is determined based on the ratio of a/b, and type of support on the plate side (boundary condition)
KNKT *Komite Nasional Keselamatan Transportasi* (Indonesian National Transportation Safety Committee)
n and *s* Direction normal to the edge and the direction parallel to the edge, respectively
v Poisson's ratio
w Transverse deflection

References
[1] A. A. Jusuf, M. Mora, Review of aircraft crashworthiness design, *Warta Ardhia: Jurnal Perhubungan Udara*, 2016, **42**, 109-116, doi: 10.25104/wa.v42i3.241.117-122.
[2] R. Rahmawati, M. Martono, R. D. Pangesti, J. Mahbub, Percentage of the number of accidents and models that cause air transportation accidents in Indonesia during the 2020 Covid pandemic. Bangun Rekaprima: Majalah Ilmiah Pengembangan Rekayasa, *Sosial dan Humaniora*, 2021, **7**, 62-70. doi: 10.32497/bangunrekaprima.v7i2,%20Oktober.2998.
[3] "Countries and regions with the highest number of fatal civil airliner accidents from 1945 through February 28, 2022," Transportation & Logistics › Aviation Statista Ltd., 2022.
[4] "Accident Statistics," International Civil Aviation Organization, ICAO, 2023.
[5] "KNKT Transportation Accident Investigation Statistics Book," National Transportation Safety Committee, KNKT, 2021.
[6] H. Ali Khan, A. Shahid, S. Khushbash, A. Hameed, S. Zameer Abbas, Investigation of failure and development of mitigation techniques of a cracked aircraft wing spar cap, *Engineering Failure Analysis*, 2023, **147**, 107149, doi: 10.1016/j.engfailanal.2023.107149.
[7] A. Hameed, A. Nawaz, H. Ali Khan, Z. Mehmood, F. Akram, Failure analysis of a cracked cylinder block assembly of an aircraft brake system, *Engineering Failure Analysis*, 2022, **133**, 105948, doi: 10.1016/j.engfailanal.2021.105948.
[8] Z. Li, X. Guo, K. Huang, W. Luo, F. Xiong, G. Zhu, Failure analysis of an Ag-Mg-Ni reed in a relay in aircraft applications, *Engineering Failure Analysis*, 2022, **131**, 105807, doi: 10.1016/j.engfailanal.2021.105807.
[9] Z. Mehmood, A. Hameed, A. Javed, A. Hussain, Analysis of premature failure of aircraft hydraulic pipes, *Engineering Failure Analysis*, 2020, **109**, 104356, doi: 10.1016/j.engfailanal.2019.104356.
[10] H. Ali Khan, W.-M. Wang, K. Wang, S. Li, S. Miller, J. Li, Investigation of mechanical behavior of dissimilar material FSBR joints exposed to a marine environment, *Journal of Manufacturing Processes*, 2019, **37**, 376-385, doi: 10.1016/j.jmapro.2018.12.011.
[11] Z. Mehmood, A. Hameed, S. Safdar, F. Siddiqui, Multiaxial stress mapping and fatigue failure prediction of aircraft hydraulic pipes, *Engineering Failure Analysis*, 2021, **121**, 105168, doi: 10.1016/j.engfailanal.2020.105168.
[12] A. S. Sayyad, Y. M. Ghugal, Bending, buckling and free vibration of laminated composite and sandwich beams: a critical review of literature, *Composite Structures*, 2017, **171**, 486-504, doi: 10.1016/j.compstruct.2017.03.053.
[13] L. Solazzi, Reliability evaluation of critical local buckling load on the thin walled cylindrical shell made of composite material, *Composite Structures*, 2022, **284**, 115163, doi: 10.1016/j.compstruct.2021.115163.
[14] R. Daya Karthic., N. Harish., R. Risheek., B. R. Lokavarapu, Non-linear buckling analysis of stiffened panel under uniaxial loading, *Materials Today: Proceedings*, 2023, doi: 10.1016/j.matpr.2023.02.046.
[15] K. Ghavami, M. Reza, Nonlinear large deflection analysis of stiffened plates, Finite Element Analysis - Applications in Mechanical Engineering: InTech, 2012.
[16] Ridwan, T. Putranto, F. B. Laksono, A. R. Prabowo, Fracture and Damage to the Material accounting for Transportation Crash and Accident, *Procedia Structural Integrity*, 2020, **27**, 38-45, doi: 10.1016/j.prostr.2020.07.006.
[17] R. Ridwan, A. R. Prabowo, N. Muhayat, T. Putranto, J. M. Sohn, Tensile analysis and assessment of carbon and alloy steels using FE approach as an idealization of material fractures under collision and grounding, *Curved and Layered Structures*, 2020, **7**, 188-198, doi: 10.1515/cls-2020-0016.
[18] A. R. Prabowo, J. M. Sohn, D. M. Bae, J. H. Cho, Performance assessment on a variety of double side structure during collision interaction with other ship, *Curved and Layered Structures*, 2017, **4**, 255-271, doi: 10.1515/cls-2017-0017.
[19] A. R. Prabowo, J. M. Sohn, Nonlinear dynamic behaviors of outer shell and upper deck structures subjected to impact loading in maritime environment, *Curved and Layered Structures*, 2019,

© Engineered Science Publisher LLC 2024

6, 146-160, doi: 10.1515/cls-2019-0012.
[20] A. R. Prabowo, T. Muttaqie, J. M. Sohn, D. M. Bae, A. Setiyawan, On the failure behaviour to striking bow penetration of impacted marine-steel structures, *Curved and Layered Structures*, 2018, **5**, 68-79, doi: 10.1515/cls-2018-0006.
[21] M. C. Xu, Z. J. Song, B. W. Zhang, J. Pan, Empirical formula for predicting ultimate strength of stiffened panel of ship structure under combined longitudinal compression and lateral loads, *Ocean Engineering*, 2018, **162**, 161-175, doi: 10.1016/j.oceaneng.2018.05.015.
[22] A. Prato, M. S. M. Al-Saymaree, C. A. Featherston, D. Kennedy, Buckling and post-buckling of thin-walled stiffened panels: modelling imperfections and joints, *Thin-Walled Structures*, 2022, **172**, 108938, doi: 10.1016/j.tws.2022.108938.
[23] M. A. G. Calle, R. E. Oshiro, M. Alves, Ship collision and grounding: scaled experiments and numerical analysis, *International Journal of Impact Engineering*, 2017, **103**, 195-210, doi: 10.1016/j.ijimpeng.2017.01.021.
[24] H. S. Alsos, J. Amdahl, O. S. Hopperstad, On the resistance to penetration of stiffened plates, Part II: numerical analysis, *International Journal of Impact Engineering*, 2009, **36**, 875-887, doi: 10.1016/j.ijimpeng.2008.11.004.
[25] Nonami R., Kitamura M., Takezawa A., S. Hirakawa, A study on optimization the structure of ship in consideration of layout of the stiffeners, 2014.
[26] D. Durban, Z. Zuckerman, Elastoplastic buckling of rectangular plates in biaxial compression/tension, *International Journal of Mechanical Sciences*, 1999, **41**, 751-765, doi: 10.1016/s0020-7403(98)00055-1.
[27] L. Belenkiy, Y. Raskin, Estimate of the ultimate load on structural members subjected to lateral loads, *Marine Technology and SNAME News*, 2001, **38**, 169-176, doi: 10.5957/mt1.2001.38.3.169.
[28] D. A. Danielson, A. Wilmer, Buckling of stiffened plates with bulb flat flanges, *International Journal of Solids and Structures*, 2004, **41**, 6407-6427, doi: 10.1016/j.ijsolstr.2004.05.063.
[29] Y. B. Kwon, H. S. Park, Compression tests of longitudinally stiffened plates undergoing distortional buckling, *Journal of Constructional Steel Research*, 2011, **67**, 1212-1224, doi: 10.1016/j.jcsr.2011.02.015.
[30] A. Prabowo, R. Ridwan, T. Muttaqie, On the resistance to buckling loads of idealized hull structures: FE analysis on designed-stiffened plates, *Designs*, 2022, **6**, 46, doi: 10.3390/designs6030046.
[31] R. Seifi, N. Khoda-yari, Experimental and numerical studies on buckling of cracked thin-plates under full and partial compression edge loading, *Thin-Walled Structures*, 2011, **49**, 1504-1516, doi: 10.1016/j.tws.2011.07.010.
[32] S. H. Sujiatanti, S. Tanaka, S. Shinkawa, Y. Setoyama, D. Yanagihara, Experimental and numerical studies for buckling and collapse behaviors of a cracked thin steel panel subjected to sequential tensile and compressive loading, *Thin-Walled Structures*, 2020, **157**, 107059, doi: 10.1016/j.tws.2020.107059.
[33] V. K. Mantzaroudis, D. G. Stamatelos, An approximate closed-form buckling solution for the local skin buckling of stiffened plates with omega stringers: the case of antisymmetric cross-ply and angle-ply laminations, *Structures*, 2020, **28**, 1196-1209, doi: 10.1016/j.istruc.2020.09.035.
[34] C. B. York, Laminate stiffness tailoring for improved buckling performance, *Thin-Walled Structures*, 2021, **161**, 107482, doi: 10.1016/j.tws.2021.107482.
[35] M. Oiwa, T. Ogasawara, H. Yoshinaga, T. Oguri, T. Aoki, Numerical analysis of face sheet buckling for a CFRP/Nomex honeycomb sandwich panel subjected to bending loading, *Composite Structures*, 2021, **270**, 114037, doi: 10.1016/j.compstruct.2021.114037.
[36] Y. Peng, Y.-E. Ma, W. Sun, W. Zhang, Z. Wang, Z. Yang, Buckling fatigue behavior of 2A97 Al-Li alloy stiffened panels under shear loading, *Engineering Failure Analysis*, 2021, **128**, 105575, doi: 10.1016/j.engfailanal.2021.105575.
[37] A. Prato, M. S. M. Al-Saymaree, C. A. Featherston, D. Kennedy, Buckling and post-buckling of thin-walled stiffened panels: modelling imperfections and joints, *Thin-Walled Structures*, 2022, **172**, 108938, doi: 10.1016/j.tws.2022.108938.
[38] T. Yao, M. Fujikubo, Buckling and Ultimate Strength of Ship and Ship-like Floating Structures. Butterworth-Heinemann, Oxford, United Kingdom, 2016.
[39] C. M. Wang, Y. P. Zhang, D. M. Pedroso, Hencky bar-net model for plate buckling, *Engineering Structures*, 2017, **150**, 947-954, doi: 10.1016/j.engstruct.2017.07.080.
[40] A. E. H. Love, The small free vibrations and deformation of a thin elastic shell, *Philosophical Transactions of the Royal Society of London (A)*, 1888, **179**, 491-546, doi: 10.1098/rsta.1888.0016.
[41] D. Quinn, A. Murphy, W. McEwan, F. Lemaitre, Stiffened panel stability behaviour and performance gains with plate prismatic sub-stiffening, *Thin-Walled Structures*, 2009, **47**, 1457-1468, doi: 10.1016/j.tws.2009.07.004.
[42] F. E. Goldarag, S. Barzegar, A. Babaei, An experimental method for measuring the clamping force in double lap simple bolted and hybrid (bolted-bonded) joints, *Transactions of FAMENA*, 2015, **39**, 87-94.
[43] F. Esmaeili-Goldarag, A. Babaei, H. Jafarzadeh, An experimental and numerical investigation of clamping force variation in simple bolted and hybrid (bolted-bonded) double lap joints due to applied longitudinal loads, *Engineering Failure Analysis*, 2018, **91**, 327-340, doi: 10.1016/j.engfailanal.2018.04.047.
[44] ANSYS. (2009). ANSYS Workbench User's Guide. ANSYS Inc., Pennsylvania, United States.
[45] Q. T. Do, T. Ghanbari-Ghazijahani, A. R. Prabowo, Developing empirical formulations to predict residual strength and damages in tension-leg platform hulls after a collision, *Ocean Engineering*, 2023, **286**, 115668, doi: 10.1016/j.oceaneng.2023.115668.
[46] M. I. Hanif, R. Adiputra, A. R. Prabowo, Y. Yamada, N. Firdaus, Assessment of the ultimate strength of stiffened panels of ships considering uncertainties in geometrical aspects: finite

 © Engineered Science Publisher LLC 2024

element approach and simplified formula, *Ocean Engineering*, 2023, **286**, 115522, doi: 10.1016/j.oceaneng.2023.115522.
[47] S. Suryanto, A. R. Prabowo, T. Muttaqie, I. Istanto, R. Adiputra, N. Muhayat, A. Fajri, M. Braun, S. Ehlers, Evaluation of high-tensile steel using nonlinear analysis: experiment-FE materials benchmarking of LNG carrier structures under low-temperature conditions, *Energy Reports*, 2023, **9**, 149-161, doi: 10.1016/j.egyr.2023.05.252.
[48] A. R. Prabowo, R. Ridwan, M. Braun, S. Song, S. Ehlers, N. Firdaus, R. Adiputra, Comparative study of shell element formulations as NLFE parameters to forecast structural crashworthiness, *Curved and Layered Structures*, 2023, **10**, 20220217, doi: 10.1515/cls-2022-0217.
[49] A. R. Prabowo, R. Ridwan, T. Tuswan, F. Imaduddin, Forecasting the effects of failure criteria in assessing ship structural damage modes, *Civil Engineering Journal*, 2022, **8**, 2053-2068, doi: 10.28991/cej-2022-08-10-03.
[50] I. B. Wiranto, S. O. Saraswati, I. R. Alfikri, C. Chairunnisa, F. C. Megawanto, M. I. Adhynugraha, N. C. Majid, Effect of Boundary Condition on Numerical Study of UAV Composite Skin Panels Under Dynamic Impact Loading, *Mekanika: Majalah Ilmiah Mekanika,* 2024, **23**, 22-32, doi: 10.20961/mekanika.v23i1.77875.
[51] R. Ridwan, S. Sudarno, H. Nubli, A. Chasan, I. Istanto, P. S. Pratama, Numerical Analysis of Openings in Stiffeners under Impact Loading: Investigating Structural Response and Failure Behavior, *Mekanika: Majalah Ilmiah Mekanika,* 2023, **22**, 115-125, doi: 10.20961/mekanika.v22i2.76774.
[52] J. H. Cho, R. Ridwan, R. P. Kusuma, J. Triyono, N. Muhayat, A. Fajri, F. B. Laksono, Design Analysis and Structural Prediction of Bus Driver Chair Support: A Study Case using HOQ and FEM, *Mekanika: Majalah Ilmiah Mekanika,* 2023, **22**, 1-12, doi: 10.20961/mekanika.v22i1.44371.

Publisher's Note: Engineered Science Publisher remains neutral with regard to jurisdictional claims in published maps and institutional affiliations.

© Engineered Science Publisher LLC 2024